学位論文

Theoretical Study
on the Foundation of Statistical Mechanics
in Isolated Quantum Systems
(孤立量子系における統計力学の基礎に関する理論的研究)

平成 26 年 12 月 博士 (理学) 申請

東京大学大学院理学系研究科
物理学専攻

池田 達彦

Abstract

Relaxation dynamics being observed in ultracold atom experiments, the foundation of statistical mechanics in isolated quantum systems has recently attracted renewed interest. The recent viewpoint of "typicality" that a vast majority of quantum states look macroscopically identical has enabled us to understand that equilibrium states, or macroscopically unchanging states, can appear even in the course of unitary time evolution. This thesis archives two original studies concerning statistical-mechanical properties of these equilibrium states.

First, we address the issue of how accurately the microcanonical ensemble can approximate those equilibrium states in small isolated quantum systems. We numerically analyze quantum quenches in a one-dimensional nonintegrable hard-core Bose-Hubbard model at the 1/3 filling with the nearest- and next-nearest-neighbor hopping and the interparticle interaction, where the number of sites L ranges from 15 to 24. We find that the accuracy of the microcanonical ensemble vanishes proportionally to D^{-1}, where D denotes the dimension of the Hilbert space. This implies that the microcanonical ensemble is quite accurate in a system already with several particles. In fact, in our model with only 8 bosons on $L = 24$ sites, the relative error is already as small as 0.01%, which will improve approximately by one order of magnitude every time we increase the number of bosons by one because D grows exponentially as L increases.

Second, we discuss the thermodynamic entropy of those equilibrium states. We point out that, in an isolated quantum system, the von Neumann entropy is inconsistent with the second law of thermodynamics since it never changes upon any unitary external operation whether or not it is quasi-static. Then, we propose the diagonal entropy, which is nothing but the Shannon entropy in the energy eigenbasis, as the right candidate for the microscopic definition of the thermodynamic entropy by showing that it is consistent with the second law of thermodynamics. Namely, assuming that a given unitary external operation is performed at time τ, which is randomly chosen, the diagonal entropy increases or stays constant upon the operation not only on average over τ but also for almost all τ.

Acknowledgements

I wish to greatly thank my PhD advisor, Professor Masahito Ueda for his advice, fruitful discussions and encouragements all over my PhD program. I would also like to thank Professor Anatoli Polkovnikov for letting me stay at Boston University and giving me a lot of advice and encouragements. Professors Shunsuke Furukawa and Yu Watanabe gave me a lot of advice on the numerical treatment of quantum many-body systems. The collaboration with Dr. Naoyuki Sakumichi has been very fruitful to improve my skill of the academic writing and mathematically rigorous treatments of physical problems. Fruitful discussions with a number of researchers have been very helpful. Especially, I wish to thank Professor Takashi Mori, Dr. Eriko Kaminishi, Dr. Michael Kolodrubetz, Dr. Luca D'Alessio, Dr. Peter Grisins, Dr. Hyungwon Kim, Mr. Yui Kuramochi, Mr. Yusuke Horinouchi, Mr. Kohaku H. Z. So, and Mr. Tomohiro Shitara. I also thank Mrs. Asako Takeuchi for helping me with paperworks and encouraging me. Finally, I greatly acknowledge the JSPS for financial support (Grant No. 248408).

Publication List

This thesis is based on the following two publications:

1. Tatsuhiko N. Ikeda and Masahito Ueda, *How accurately can the microcanonical ensemble describe small isolated quantum systems?*, in preparation.

2. Tatsuhiko N. Ikeda, Naoyuki Sakumichi, Anatoli Polkovnikov, and Masahito Ueda, *The Second Law of Thermodynamics under Unitary Evolution and External Operations*, Annals of Physics 354, 338 (2015).

The following five publications are not directly related to this thesis.

1. Yu Watanabe and Tatsuhiko N. Ikeda, *Analysis of relaxation time scales in isolated quantum systems by using band random matrices*, in preparation.

2. Eriko Kaminishi, Takashi Mori, Tatsuhiko N. Ikeda, and Masahito Ueda, *Entanglement prethermalization: Locally thermal but non-locally non-thermal states in a one-dimensional Bose gas*, submitted to Nature Physics [preprint, arXiv:1410.5576].

3. Hyungwon Kim, Tatsuhiko N. Ikeda, and David A. Huse, *Testing whether all eigenstates obey the Eigenstate Thermalization Hypothesis*, Physical Review E 90, 052105 (2014).

4. Tatsuhiko N. Ikeda, Yu Watanabe, and Masahito Ueda, *Finite-size scaling analysis of the eigenstate thermalization hypothesis in a one-dimensional interacting Bose gas*, Physical Review E 87, 012125 (2013).

5. Tatsuhiko N. Ikeda, Yu Watanabe, and Masahito Ueda, *Eigenstate Randomization Hypothesis: Why Does the Long-Time Average Equal the Microcanonical Average?*, Physical Review E 84, 021130 (2011).

Contents

Chapter 1

Introduction

1.1 Statistical mechanics and its presuppositions

Statistical Mechanics is a theory in physics to calculate the "properties" of macroscopic objects at thermal equilibrium[1] [1, 2] from the knowledge of the constituent atoms and molecules. Here we mean by the "properties" (i) the thermodynamic functions such as the entropy and the free-energy [3] and (ii) the correlation functions of the constituent particles such as the spin-spin correlations in lattice systems and the momentum distribution of molecules in a gas. Once we know what the constituent particles are and how they interact with each other, (i) and (ii) can be calculated in principle through a procedure that statistical mechanics gives. Statistical mechanics has been successfully applied to a wide range of systems such as gases [4], magnets [5], and even stars [6].

Statistical mechanics is constructed from the following two presuppositions on thermal equilibrium states in isolated systems [7]. One presupposition is that we can calculate physical quantities of an isolated system at thermal equilibrium by using the microcanonical ensemble, which is a statistical model in which every microstate at a given energy appears with equal probability. The other is that the thermodynamic entropy S of a thermal equilibrium state of an isolated system is given by Boltzmann's formula, $S = k_{\rm B} \ln W$, where $k_{\rm B}$ and W are Boltzmann's constant and the number of microstates that has the given energy. Once we admit these presuppositions, all the properties (i) and (ii) described above can be derived with the help of thermodynamics. As for the property (i) defined above, the entropy S is given directly by Boltzmann's formula [2] and Helmholtz' free-energy F is derived as $F = E - TS$

[1] In this thesis, statistical mechanics does not imply nonequilibrium statistical mechanics but equilibrium statistical mechanics.

from thermodynamics, where E and T are the internal energy and the temperature of the system. As for the property (ii) defined above, we can calculate any correlation functions by invoking the microcanonical ensemble.

Those two presuppositions also allow us to calculate the properties (i) and (ii) of thermal equilibrium states of a system in contact with a heat bath [2]. In fact, by applying the microcanonical ensemble to the total isolated system of the system and the bath, we obtain the canonical ensemble that describes the system of interest. The grand canonical ensemble is also obtained in a similar way.

However, those two presuppositions have not yet been derived from the first principle even though the great success of statistical mechanics is undebatable. It is well known that Boltzmann himself, the inventor of statistical mechanics, could not finally justify those two presuppositions. Some researchers followed Boltzmann to solve this problem from the viewpoint of ergodicity [8]. The ergodicity [9] is a property of a class of classical-mechanical systems that an initial state travels every microstates with equal probability in the course of time evolution, whereby the long-time average of a physical quantity is guaranteed to be equal to its microcanonical ensemble average. It has been shown that there are systems showing ergodicity such as Sinai's billiard [10]. Nevertheless, it has recently been pointed out that the ergodicity cannot be the foundation of statistical mechanics even though it stimulated fruitful mathematical research [11, 7, 12]. This is because the ergodicity requires an exponentially long time average, which is typically longer than the age of the universe, while what we observe in reality is physical quantities at each instant of time.

1.2 Typicality of thermal microstates

Recently, another picture of thermal equilibrium states, instead of the ergodicity, has attracted attention and the foundation of statistical mechanics has been reexamined from this point of view. Namely, almost all microstates, or typical microstates, themselves macroscopically look like thermal equilibrium states on a given energy surface [13, 14, 15, 16] This idea of typicality of thermal equilibrium states can be envisaged in classical N particles, or a gas, confined in a container. Each microstate corresponds to a set of coordinates and momenta of the N particles. Let us consider, for example, the number of particles in the half of the container. Then, if N is much larger than unity, it is given approximately by $N/2$ for almost all of the microstates, which is the expectation value in the thermal equilibrium state. The typicality is the idea that almost every microstate itself looks thermal in all likelihood with no averaging process

required.

As we review in Chapter 2 in detail, the typicality of thermal equilibrium states has recently been shown in isolated quantum systems [14, 13, 15]. Although similar ideas had already been obtained much earlier [17, 18], they seemed not to be widely accepted at that time. In addition, the typicality appears more prominently in quantum systems than in classical ones. Thus we focus on quantum systems throughout this thesis.

With the viewpoint of the typicality, we can avoid the unrealistically long time that the ergodicity approach requires to justify the usage of the microcanonical ensemble [19, 20, 21, 22, 23]. This is because, according to this picture of "typicality", thermal equilibration is regarded as an escape from an atypical region in which a state out of equilibrium initially resides,and the process can occur in a time much shorter than the time needed for the state to travel all over the microstates. This scenario is formulated more precisely in Chapter 3.

According to this picture, the microcanonical ensemble average is just a mathematical trick to extract the information about the thermal equilibrium state that is shared by almost all the microstates. We note that other assignments of probability on the microstates would thus also work just as the microcanonical ensemble does, while the equal probability in the microcanonical ensemble plays an crucial role in the ergodicity [16].

1.3 Experiments with ultracold atomic gases

Yet another important reason why the foundation of statistical mechanics has recently attracted considerable attention is that isolated quantum systems have been realized experimentally by using ultracold atomic gases [24, 25, 26, 27]. The temperature of these gases reaches no higher than 100nK by magnetically and optically trapping thermal atoms in a high vacuum and cooling them down by laser and evaporative cooling techniques [28]. At this extremely low temperature, Bose gases such as ^{87}Rb and ^{23}Na exhibit Bose-Einstein condensation [29, 30]. Namely, degenerate ultracold atomic gases are macroscopic objects showing the quantum nature. Furthermore, by using optical techniques, ultracold atomic gases can be confined into lower dimensional systems including the zero-dimensional ones, or lattice systems [31, 32, 33]. Due to the flexibility in manipulation and the quantum nature of the system, ultracold atoms are regarded as promising candidates for quantum simulators [34, 35]

Thermalization under unitary time evolution has been observed with ^{87}Rb atoms in a one-dimensional lattice system by Trotzky and co-workers [36]. They have created an ultracold ^{87}Rb atoms in a one-dimensional lattice and succeeded in preparing such an initial state out

of equilibrium that every second site of the lattice, or every "even" site, is occupied by one ^{87}Rb by using a bichromatic optical superlattice. They have observed the time evolution of the number density of the "odd" sites and shown that it shows thermal equilibration. They have also shown that the time evolution is well described by the unitary time evolution according to a Hamiltonian. Thus their study is also significant to have directly demonstrated that an ultracold atomic system actually evolves according to the unitary evolution.

Experiments in ultracold atoms not only confirm thermal equilibration in isolated quantum systems but also explore non-thermal stationary states in those systems, which elucidate the necessary condition for the applicability of the standard statistical mechanics. Kinoshita and co-workers have investigated a "quantum Newton's cradle", which is a 1D ^{87}Rb gas along which an anharmonic potential is imposed [37]. They have prepared an initial state out of equilibrium by creating a superposition of left and right moving atomic clouds. They have found that the momentum distribution does not become thermal, or the Bose-Einstein distribution, but relaxes to a non-thermal distribution since the 1D Bose gas is approximately described by the Lieb-Linger model, which is integrable. It has been indicated that the Hamiltonian should be nonintegrable for thermalization to occur. Gring and co-workers have observed prethermalization by coherently splitting a 1D Bose gas, which is approximately described by an integrable model, namely, the Tomonaga-Luttinger liquid [38]. Prethermalization is a relaxation to a non-thermal quasi-stationary state before reaching the thermal equilibrium state [39]. In this experimental setup, it has also been shown that prethermalization occurs so as to exhibit a light-cone structure in space [40].

We note that isolated quantum systems with a small and definite number of fermions have been realized [41], whereas the experiments reviewed above involve more than a hundred particles in the systems. Thus it is now feasible to investigate how thermalization behavior changes and statistical mechanics works better as the system size increases starting from a few-body system.

As highlighted above, the foundation of statistical mechanics is now also addressable not only theoretically but also experimentally. Now that thermalization has been shown to occur in reality, it is an urgent task to give theoretical explanations on the phenomenon from quantum mechanics. On the other hand, the above experiments in nearly integrable systems show that relaxation in isolated quantum systems has a richer structure depending on the feature of the microscopic models. To understand non-thermal stationary states has also attracted much attention.

1.4 Organization of this thesis

In this thesis, we discuss the two presuppositions, introduced in Sec. 1.1, of statistical mechanics in isolated quantum systems from a viewpoint of the typicality of thermal equilibrium states. In Chapter 2, we review the typicality of thermal pure states by giving a mathematical proof following Ref. [15]. We see that even a single pure state can represent a thermal equilibrium state as long as only few-body observables are concerned. In Chapter 3, we review how equilibration, or appearance of stationary states, is formulated under a unitary time evolution along with the idea of the typicality. We also introduce the eigenstate thermalization hypothesis (ETH), which dictates that every energy eigenstate in a small energy window looks the same in the thermodynamic limit. The ETH is widely accepted as the underlying mechanism for the stationary state that is reached during the unitary time evolution to be well described by the microcanonical ensemble. Chapters 4 and 5 respectively concern the two presuppositions described in Sec. 1.1 based on the author's original results. In Chapter 4, we address the issue of *how accurately* the microcanonical ensemble works in small isolated quantum systems rather than *why* it does in the thermodynamic limit that previous studies have addressed. We show that the accuracy of the microcanonical ensemble improves proportionally to $1/D$ where D represents the dimension of the Hilbert space, which grows exponentially with the number of particles of the system. In Chapter 5, we discuss the microscopic definition of the thermodynamic entropy of stationary states including pure states rather than the thermodynamic entropy of the microcanonical ensemble. We show that the diagonal entropy [42], which is the Shannon entropy in the energy eigenbasis, increases upon any unitary external operation consistent with the second law of thermodynamics. Chapter 6 is devoted to the summary of the discussions in this thesis and makes some remarks on the future prospect. The relations between the chapters are shown in Fig. 1.1

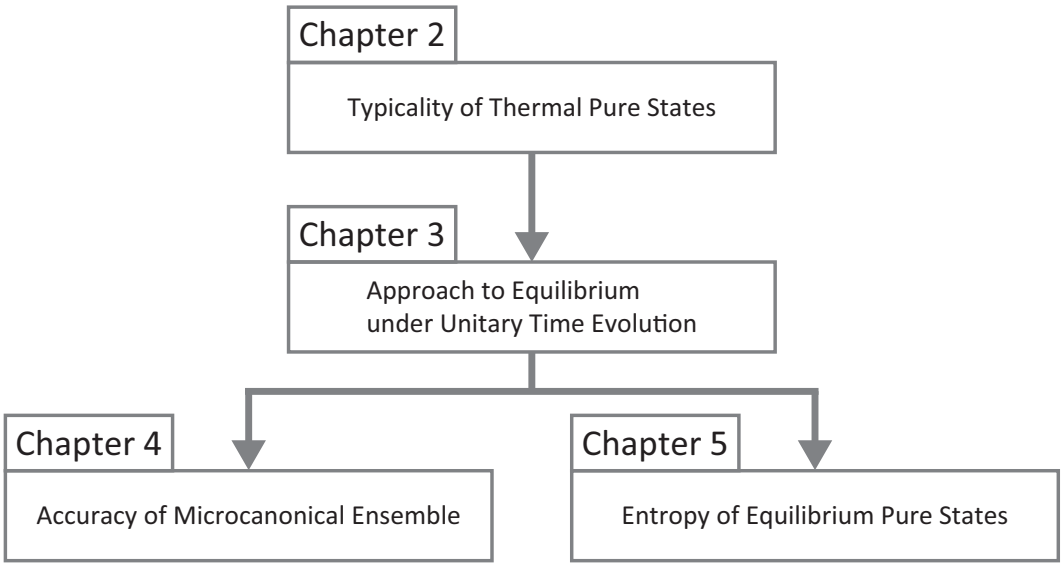

Figure 1.1: The relations between the chapters.

Chapter 2

Typicality of Thermal Pure States

The microcanonical ensemble is constituted of a set of pure states that are averaged to calculate the expectation values of observables of interest at thermal equilibrium. Recently, it has been shown that averaging is not necessary and almost all pure states in the ensemble are thermal states by themselves. This remarkable property is called the "typicality" of thermal pure states, which was discovered by several different groups independently [14, 13, 15]. In this chapter, we review the typicality due to Sugita [15].

2.1 A parable in classical mechanics

The typicality of thermal states can be envisaged in classical mechanics. Let us consider a gas consisting of N particles in a container, which is symmetric in the left and right when cut into halves. In classical mechanics, every microstate of the gas is represented by the set of the positions and the momenta that corresponds to a point in the phase space.

The microcanonical ensemble is the statistical ensemble in which each microstate having a given energy appears with equal probability. According to statistical mechanics, the expectation value of an observable at thermal equilibrium is calculated by averaging over the ensemble. For example, the observable of the number of particles in the left half of the container would approximately give $N/2$ due to the symmetry under the interchange of the two halves of the container. Here we assume that the Hamiltonian is also symmetric.

However, the average is not essential to obtain $N/2$ if N is quite large. Based on the law of large numbers, it is natural to expect that most microstates themselves approximately give $N/2$ for the observable. The fraction of the microstates that deviate from the average decreases as $N^{-1/2}$ and vanishes in the thermodynamic limit. This is the basic idea behind the

typicality of thermal states: even a single microstate in the microcanonical ensemble gives essentially the same physical quantities as does their average.

In our example of classical mechanics, the typicality can be seen because the observable is extensive or proportional to N. If we take non-extensive observables such as the number of particles in an area with a finite volume independent of the system size, the typicality does not apply because the fluctuation of the observable from one microstate to another stays constant as N increases.

The typicality emerges more dramatically in quantum mechanics as we show in the next section. The typicality is seen for all few-body observables including local ones. Furthermore, unlike the above example, the fraction of atypical states decays exponentially in the system size.

2.2 Typicality in lattice quantum systems

2.2.1 Model

We consider a lattice quantum system of N sites. The Hilbert space of the total system $\mathcal{H}$ is given by the direct products of the Hilbert space of every site $\mathcal{H}_i$, where $i = 1, 2, \ldots, N$ labels the sites. We assume that all $\mathcal{H}_i$ are identical and denote their dimensions by d_S: $\dim \mathcal{H}_i = d_S$ $(i = 1, 2, \ldots, N)$. Then the dimension of $\mathcal{H}$ is given by $\dim \mathcal{H} \equiv D = d_S^N$. For the spin-1/2 lattice systems, we have $d_S = 2$ and $D = 2^N$.

To consider physical observables, we introduce the basis set of Hermitian operators acting on $\mathcal{H}$. First we denote by $\{\hat{a}_i^\alpha\}_{\alpha=0}^{d_S^2-1}$ a basis set of Hermitian operators acting on $\mathcal{H}_i$ that is the set of the generators of the unitary group of degree d_S. In particular, $\hat{a}_i^0$ is chosen to be the identity operator and the orthonormality condition is given by

$$\mathrm{tr}_{\mathcal{H}_i}\left[\hat{a}_i^\alpha \hat{a}_i^\beta\right] = d_S \delta_{\alpha\beta}. \tag{2.1}$$

For $d_S = 2$, the basis set reads $\hat{a}_i^0 = 1_{2\times 2}$ and $\hat{a}_i^\alpha = \hat{\sigma}^\alpha$ $(\alpha = 1, 2, 3)$, where $\hat{\sigma}^\alpha$'s are the Pauli matrices. Second these basis sets lead to the basis set of the Hermitian operators acting on $\mathcal{H}$ through the (direct) products:

$$\hat{A}(\{\alpha_i\}) = \prod_{i=1}^{N} \hat{a}_i^{\alpha_i}. \tag{2.2}$$

The orthonormality condition for the basis is given by

$$\mathrm{tr}\left[\hat{A}(\{\alpha_i\})\hat{A}(\{\beta_i\})\right] = d_S^N \prod_{i=1}^{N} \delta_{\alpha_i\beta_i}. \tag{2.3}$$

We note that our normalization of the basis is convenient for discussing the system size dependence. In fact, when we consider, for $d_S = 2$, the z-component of the spin at $i = 1$, it is represented by the operator σ_1^z for $N = 1$ and by $\sigma_1^z \otimes 1 \otimes \cdots$ for $N \geq 2$, both of which are the members of our basis set. If our normalization were Eq. (2.1) without d_S on the right-hand side, the member of the basis set corresponding to the z-component of the spin at $i = 1$ would be $2^{-N}\sigma_1^z \otimes 1 \otimes \cdots$.

Now we define few-body observables that are the key to understanding thermal pure states. From the operators of the form of Eq. (2.2), we take the ones in which α_i takes nonzero values for M values of i and zero otherwise. An observable is defined to be M-body if it can be represented by a linear combination of such operators. Thus the 0-body observable should be proportional to the identity operator. In spin systems, for example, the magnetization $\sum_i S_i^z$ is one-body and the Heisenberg Hamiltonian $\sum_{\langle i,j\rangle} \mathbf{S}_i \cdot \mathbf{S}_j$ is two-body, where $\sum_{\langle i,j\rangle}$ denotes the sum over adjacent sites on the lattice. All observables that we usually consider in thermodynamic systems are few-body observables. We note that the set of the M-body observables form a vector space and its dimension is $\binom{N}{M}(d_S^2-1)^M$, which is much smaller compared with the total number of the basis of the Hermitian operators acting on $\mathcal{H}$ which is given by d_S^N. This is because the former grows as N^M, whereas the latter grows exponentially in N.

The Hamiltonian $\hat{H}$ is an arbitrary Hermitian operator acting on $\mathcal{H}$, which may or may not be integrable. We denote by $\{E_n\}_{n=1}^D$ the eigenbasis set of $\hat{H}$ with eigenenergies $\{E_n\}_{n=1}^D$: $\hat{H}\,|E_n\rangle = E_n\,|E_n\rangle$ $(n = 1, 2, \ldots, D)$. As discussed below, the typicality is a mathematical consequence that holds quite generally. Whether the thermal state thus derived is actually reached in time evolution, however, is another problem which is to be discussed in Chapter 3.

2.2.2 Typical states in a microcanonical shell

The typicality is defined on the microcanonical shell $\mathcal{S}$, which is the set of energy eigenstates whose eigenenergies lie in a given energy window $[E - \delta_{\mathrm{mic}}, E + \delta_{\mathrm{mic}}]$:

$$\mathcal{S} = \{\, n \mid E - \delta_{\mathrm{mic}} \leq E_n \leq E + \delta_{\mathrm{mic}}\}. \tag{2.4}$$

We denote by d the number of energy eigenstates in the microcanonical shell. We also define the shell Hilbert space as

$$\mathcal{H}_{\rm mic} = \left\{ |\psi\rangle = \sum_{n\in\mathcal{S}} c_n |E_n\rangle \;\middle|\; c_n \in \mathbb{C},\ \forall n \in \mathcal{S};\ \sum_{n\in\mathcal{S}} |c_n|^2 = 1 \right\}. \tag{2.5}$$

This is equivalent to S^{2d-1} by definition.

We define the uniform Haar measure on $\mathcal{H}_{\rm mic}$ as,

$$P(\{c_n\}) \prod_{n\in\mathcal{S}} {\rm dRe}c_n {\rm dIm}c_n \propto \delta\left(\sum_{n\in\mathcal{S}} |c_n|^2 - 1\right) {\rm dRe}c_n {\rm dIm}c_n. \tag{2.6}$$

This is invariant under any unitary transformation U: $\mathbf{c} \to U\mathbf{c}$. This property leads to the following two formulae, with which we show the typicality.

Lemma 1. We have

$$\overline{c_m c_n^*} = \frac{1}{d}\delta_{mn}; \tag{2.7}$$

$$\overline{c_k c_l^* c_m c_n^*} = \frac{1}{d(d+1)}(\delta_{kl}\delta_{mn} + \delta_{km}\delta_{ln}), \tag{2.8}$$

where $\overline{\cdots}$ denotes the average according to the uniform Haar measure (2.6).

Proof. As for Eq. (2.7), we introduce $A_{mn} \equiv \overline{c_m c_n^*}$. From the invariance of the uniform Haar measure under an arbitrary unitary transformation, we have $A = UAU^\dagger$ for any unitary matrix U. This implies that A is proportional to the identity matrix: $A_{mn} = ({\rm const.})\delta_{mn}$. The constant turns out to be equal to d^{-1} from the normalization condition $1 = \overline{\sum_{n\in\mathcal{S}} |c_n|^2} = ({\rm const.})d$.

As for Eq. (2.8), we have $\overline{c_k c_l^* c_m c_n^*} = C_1\delta_{kl}\delta_{mn} + C_2\delta_{km}\delta_{ln}$ from the invariance of the uniform Haar measure under any unitary transformation. Yet another symmetry under the interchanges of $k \leftrightarrow m$ and $l \leftrightarrow n$ leads to $C_1 = C_2 \equiv C$. The constant C is determined by summing both sides of $\overline{c_k c_l^* c_m c_n^*} = C(\delta_{kl}\delta_{mn} + \delta_{km}\delta_{ln})$ over k, l, m, and n under the constraints of $k = l$ and $m = n$, which reads $1 = d(d+1)C$. □

The key to deriving the typicality is that the standard deviations of the expectation values of few-body observables quickly decay as d increases. Let us take an arbitrary observable $\hat{O}$ and consider the expectation value $\langle\psi|\hat{O}|\psi\rangle$ for $|\psi\rangle \in \mathcal{H}_{\rm mic}$. First, we evaluate the average of

$\langle\psi|\hat{O}|\psi\rangle$ over all $|\psi\rangle \in \mathcal{H}_{\rm mic}$ taken according to the uniform Haar measure:

$$\overline{\langle\psi|\hat{O}|\psi\rangle} = \sum_{(m,n)\in\mathcal{S}\times\mathcal{S}} \overline{c_m^* c_n}\, \langle E_m|\hat{O}|E_n\rangle\,, = \frac{1}{d}\sum_{n\in\mathcal{S}} \langle E_n|\hat{O}|E_n\rangle = \mathrm{tr}\left[\hat{\rho}_{\rm mic}(E)\hat{O}\right]. \tag{2.9}$$

where $\hat{\rho}_{\rm mic}(E)$ denotes the microcanonical ensemble. This implies that the microcanonical ensemble can be regarded as the average over all pure states in $\mathcal{H}_{\rm mic}$ whereas it is considered as the one over the energy eigenstates. As for the variance, the following theorem holds.

Theorem 1. The variance of the expectation value of $\hat{O}$ is bounded from above as

$$\overline{[\langle\psi|\hat{O}|\psi\rangle - \overline{\langle\psi|\hat{O}|\psi\rangle}]^2} \leq \frac{\|\hat{O}\|_{\rm op}^2}{d+1}, \tag{2.10}$$

where $\|\hat{O}\|_{\rm op}$ denotes the operator norm of $\hat{O}$ that equals the maximum absolute value of the eigenvalues of $\hat{O}$.

Proof. The left-hand side of Eq. (2.10) can be estimated, with $O_{mn} \equiv \langle E_m|\hat{O}|E_n\rangle$, as

$$\begin{aligned}
\overline{[\langle\psi|\hat{O}|\psi\rangle - \overline{\langle\psi|\hat{O}|\psi\rangle}]^2} &= \sum_{\substack{(k,l,m,n)\in\mathcal{S}^4\\ k\neq l, m\neq n}} \overline{c_k^* c_l c_m c_n^*} O_{kl} O_{mn}^* && (2.11)\\
&= \frac{1}{d(d+1)} \sum_{\substack{(k,l,m,n)\in\mathcal{S}^4\\ k\neq l, m\neq n}} (\delta_{kl}\delta_{mn} + \delta_{km}\delta_{ln}) O_{kl} O_{mn}^* && (2.12)\\
&= \frac{1}{d(d+1)} \sum_{\substack{(m,n)\in\mathcal{S}^2\\ m\neq n}} |O_{mn}|^2 && (2.13)\\
&\leq \frac{1}{d(d+1)} \sum_{(m,n)\in\mathcal{S}^2} |O_{mn}|^2 && (2.14)\\
&\leq \frac{1}{d(d+1)} \sum_{m\in\mathcal{S}}\sum_{n} |O_{mn}|^2 && (2.15)\\
&= \frac{1}{d(d+1)} \sum_{m\in\mathcal{S}} \langle E_m|\hat{O}^2|E_m\rangle && (2.16)\\
&\leq \frac{\|\hat{O}\|_{\rm op}^2}{d+1}. && (2.17)
\end{aligned}$$

Here we invoked Eq. (2.8) , the completeness relation $1 = \sum_n |E_n\rangle\langle E_n|$, and $\langle\phi|\hat{O}|\phi\rangle \leq \|\hat{O}\|_{\rm op}$ ($\forall\,|\phi\rangle \in \mathcal{H}$) to obtain Eq. (2.12), Eq. (2.16), and Eq. (2.17), respectively. □

If $\hat{O}$ is a few-body observable, Theorem 1 implies that the variance of the expectation value is exponentially small in N. First we consider, for a positive integer M independent of N, an M-body observable $\hat{O}$ which has the form of Eq. (2.2). Then we have $\|\hat{O}\|_{\rm op} \leq d_S^{M/2}$ because the number of nonzero components in $\{\alpha_i\}$ is M, each $\hat{a}_{\alpha_i}$ is normalized as $\|\hat{a}_{\alpha_i}\|_{\rm hs} \equiv \sqrt{{\rm tr}[(\hat{a}_{\alpha_i})^2]} = d_S^{1/2}$, and $\|\hat{a}_{\alpha_i}\|_{\rm op} \leq \|\hat{a}_{\alpha_i}\|_{\rm hs}$, where $\|\hat{a}_{\alpha_i}\|_{\rm hs}$ is the Hilbert-Schmidt norm. Since d increases exponentially in N, the upper bound in Eq. (2.10) decays exponentially for our $\hat{O}$. Second we consider an arbitrary M-body observable which is expressed as a linear combination of the M-body observables of the form of Eq. (2.2). We assume that the coefficients in the linear combination are independent of N similarly to the Heisenberg Hamiltonian. Then, using the triangular inequalities, we have $\|\hat{O}\|_{\rm op} \leq$ (const.)$\binom{N}{M}(d_S^2-1)^M d_S^{M/2} \sim N^M$ for $N \gg 1$. Thus the upper bound in Eq. (2.10) decays exponentially for any M-body observable when we increase N with M fixed. We note that the assumption that the coefficients of the linear combination are independent of N is not essential and they can be algebraically dependent of N.

The result that the variance of the expectation value is vanishingly small implies that almost all pure states look the same as the microcanonical ensemble. In fact, Chebyshev's inequality leads to

$$\text{Prob}\left(\left|\langle\psi|\hat{O}|\psi\rangle - {\rm tr}[\hat{\rho}_{\rm mic}(E)\hat{O}]\right| \geq \epsilon\right) \leq \frac{\|\hat{O}\|_{\rm op}^2}{\epsilon^2(d+1)} \tag{2.18}$$

for any $\epsilon(>0)$. We take, for example, $\epsilon = d^{-1/3}$ then it follows that the fraction of the pure states that deviate from the microcanonical ensemble by an exponentially small distance decreases exponentially as the system size increases. Thus we conclude that almost all pure states taken from $\mathcal{H}_{\rm mic}$ according to the uniform Haar measure look like a microcanonical ensemble in the sense that they give the same expectation values for any few-body observables as does the microcanonical ensemble.

2.2.3 Canonical typicality

As a corollary of the results in the previous section, we show the canonical typicality, which dictates that most pure states in $\mathcal{H}_{\rm mic}$ look like the canonical ensemble when we look only at a subsystem in the entire lattice. This follows from the fact that all the observables in the subsystem are few-body observables.

We consider the entire lattice system consisting of a system S of interest and the rest B. Meanwhile, we have $\mathcal{H} = \mathcal{H}_S \otimes \mathcal{H}_B$ with $\mathcal{H}_S = \otimes_{i\in S}\mathcal{H}_i$ and $\mathcal{H}_B = \otimes_{i\in B}\mathcal{H}_i$. We denote by

N_S the number of the lattice points in S and then $\dim \mathcal{H}_S = d_S^{N_S} \equiv D_S$. All the information about a density matrix $\hat{\rho}$ regarding the system S are involved in the reduced density matrix $\hat{\rho}_S = \mathrm{tr}_B \hat{\rho}$ because all observables regarding the system of interest have the form of $\hat{O} \otimes 1_B$, and $\mathrm{tr}_S[\hat{\rho}_S \hat{O}] = \mathrm{tr}[\rho(\hat{O} \otimes 1_B)]$ holds for any $\hat{O}$ acting on $\mathcal{H}_S$, where 1_B is the identity operator acting on $\mathcal{H}_B$.

The reduced density matrices for $|\psi\rangle \in \mathcal{H}_{\mathrm{mic}}$ and $\overline{|\psi\rangle\langle\psi|}$ are almost the same for most $|\psi\rangle \in \mathcal{H}_{\mathrm{mic}}$. To show this result, we consider the distance between $\hat{\rho}_S^{\psi} = \mathrm{tr}_B[|\psi\rangle\langle\psi|]$ and $\hat{\sigma} = \mathrm{tr}_B[\overline{|\psi\rangle\langle\psi|}]$ defined as

$$\|\hat{\rho}_S^{\psi} - \hat{\sigma}\|_{\mathrm{hs}}^2 = \mathrm{tr}_S[(\hat{\rho}_S^{\psi} - \hat{\sigma})^2]. \tag{2.19}$$

We expand the matrix $\hat{\rho}_S^{\psi} - \hat{\sigma}$ in terms of the basis set

$$\{\hat{A}_S(\{\alpha_i\}) = \prod_{i \in S} \hat{a}_i^{\alpha_i} \mid 0 \le \alpha_i \le d_S^2 - 1 (\forall i \in S)\} \tag{2.20}$$

that satisfies the orthonormality condition $\mathrm{tr}_S[\hat{A}_S(\{\alpha_i\}\hat{A}_S(\{\beta_i\}] = D_S \prod_{i \in S} \delta_{\alpha_i \beta_i}$ and thereby obtain

$$\overline{\|\hat{\rho}_S^{\psi} - \hat{\sigma}\|_{\mathrm{hs}}^2} = D_S^{-1} \sum_{\hat{A}_S} \overline{\left(\mathrm{tr}_S[\hat{\rho}_S^{\psi}\hat{A}_S] - \mathrm{tr}_S[\hat{\sigma}\hat{A}_S]\right)^2} \tag{2.21}$$

$$= D_S^{-1} \sum_{\hat{A}_S} \overline{\left(\langle\psi|\hat{A}_S \otimes 1_B|\psi\rangle - \overline{\langle\psi|\hat{A}_S \otimes 1_B|\psi\rangle}\right)^2} \tag{2.22}$$

$$\le D_S^{-1} \sum_{\hat{A}_S} \frac{\|\hat{A}_S\|_{\mathrm{op}}}{d+1} \tag{2.23}$$

$$\le D_S^{-1} D_S^2 \frac{D_S}{d+1} \tag{2.24}$$

$$= \frac{D_S^2}{d+1}. \tag{2.25}$$

Here we have used Theorem 1 and $\|\hat{A}_S\|_{\mathrm{op}} \le \|\hat{A}_S\|_{\mathrm{hs}} = D_S^{1/2}$ to obtain Eqs. (2.23) and (2.24), respectively. If the system S is small and $N_S/N \ll 1$ for a sufficiently large N, then the upper bound (2.25) decays exponentially as N increases, which implies that the reduced density matrices of most $|\psi\rangle \in \mathcal{H}_{\mathrm{mic}}$ look the same as $\hat{\sigma}$.

In a thermodynamically normal lattice system, $\hat{\sigma}$ is the canonical ensemble since it is the reduced density matrix of the microcanonical ensemble and the standard textbook argument

applies [2]. The outline of the argument is as follows. Let us calculate the probability for the system of interest having an energy ϵ in the microcanonical ensemble with energy E. Since every microstate appears equally likely, the probability is proportional to the number of the microstates of the rest B of the system that have the energy $E - \epsilon$. The number is given by $\mathrm{e}^{S_B(E-\epsilon)} \propto \mathrm{e}^{-\beta\epsilon}$ where S_B denotes the entropy of B and $\beta \equiv \mathrm{d}S_B/\mathrm{d}E$ is the inverse temperature.

In conclusion, almost all pure states taken from the shell Hilbert space (2.5) according to the uniform Haar measure (2.6) look like the canonical ensemble when we look at a small subsystem. Here the inverse temperature is determined by the total energy set in the microcanonical shell.

2.3 Remarks

Quite recently, it has been demonstrated that quantum entanglement plays an important role in the canonical typicality [14]. If the quantum state of the total system is a direct product $|\psi\rangle = |\phi_S\rangle \otimes |\phi_B\rangle$, the reduced density matrix on the system S is $|\phi_S\rangle \langle\phi_S|$ that is pure and far from the canonical ensemble. Thus the canonical typicality implies that most pure states in the shell Hilbert space (2.5) are entangled. Moreover, since the canonical ensemble maximizes the von Neumann entropy when energy is constrained, those states are actually maximally entangled [43].

The typicality is also useful in numerical calculations. One can obtain physical quantities at thermal equilibrium by considering only a single pure state instead of taking the statistical ensemble averages. It is a nontrivial task but feasible to realize the uniform Haar measure on the shell Hilbert space with a specified energy without diagonalizing the Hamiltonian [44, 45]. According to a similar idea, the typicality-based algorithms are developed for calculating unitary time evolution [46] and the eigenstate thermalization hypothesis (ETH) [47, **?**] (see Section 3.3.1 as for the ETH).

However, regarding the foundation of statistical mechanics, the typicality itself is not fully satisfactory because the uniform Haar measure is not achievable in time evolution. According to the unitary time evolution, $|\psi\rangle = \sum_{n\in S} c_n |E_n\rangle$ in Eq. (2.5) evolves as $|\psi(t)\rangle = \sum_{n\in S} c_n \mathrm{e}^{-\mathrm{i}E_n t} |E_n\rangle$ and the weight on each energy eigenstate $|c_n|^2$ is invariant for all $n \in S$. Thus the set of the physically allowed states has zero measure in $\mathcal{H}_{\mathrm{mic}}$ and the typical state seen in time evolution, or the stationary state, is not necessarily equal to that in $\mathcal{H}_{\mathrm{mic}}$. In fact, we encounter both thermal and non-thermal stationary states depending on the characteris-

tics of the system, which is the subject reviewed in the next chapter. In Chapter 5, we show that one can define an entropy for equilibrium pure states consistently with the second law of thermodynamics from the very fact that the physically allowed states in time evolution are restricted to a small subspace in $\mathcal{H}_{\mathrm{mic}}$.

Chapter 3

Approach to Equilibrium under Unitary Time Evolution

In the previous chapter, we have learned that most pure states look thermal when taken according to the uniform Haar measure on the microcanonical shell. In this chapter, we consider a more physical measure, the time evolution, instead of the Haar measure. We show that the system reaches an effective stationary state if numerous energy eigenstates are involved and the energy spectrum is complex enough. Then we review recent studies on how the stationary state looks like depending on the characteristics of the system such as the integrability and the localization.

3.1 Unitary time evolution and quasi-periodicity

A system cannot converge to a stationary state under unitary time evolution. Let us consider an isolated quantum system associated with a D-dimensional Hilbert space $\mathcal{H}$. For simplicity, we assume that D is finite. Time evolution of an initial pure state $|\psi_0\rangle$ according to a Hamiltonian $\hat{H}$ is given by $|\psi(t)\rangle = \hat{\mathcal{U}}(t)\,|\psi_0\rangle$, where $\hat{\mathcal{U}}(t) \equiv \mathrm{e}^{-\mathrm{i}\hat{H}t}$ and the Planck constant divided by 2π is set to unity throughout this chapter. We denote by $\{|E_n\rangle\}_{n=1}^{D}$ the eigenstates of $\hat{H}$ with eigenenergies $\{E_n\}_{n=1}^{D}$, which are assumed to be discrete: $\hat{H}\,|E_n\rangle = E_n\,|E_n\rangle$. In the energy eigenbasis, the time evolution is represented by

$$|\psi(t)\rangle = \sum_{n=1}^{D} c_n \mathrm{e}^{-\mathrm{i}E_n t}\,|E_n\rangle\,, \tag{3.1}$$

where $c_n \equiv \langle E_n|\psi_0\rangle$ $(n = 1, 2, \ldots, D)$. It directly follows from Eq. (3.1) that $|\psi(t)\rangle$ never converges to a stationary state in the limit of $t \to \infty$ and each phase factor $\mathrm{e}^{-\mathrm{i}E_n t}$ keeps oscillating with the corresponding eigenenergy.

In particular, the time evolution (3.1) becomes periodic including the overall phase[1] under a certain condition that we derive as follows. We assume that not all eigenenergies $\{E_n\}_{n=1}^D$ are equal to zero because, otherwise, no time evolution occurs. Then, we have at least one nonzero eigenenergy and let it be E_1 without loss of generality. The necessary and sufficient condition for Eq. (3.1) to be periodic including the overall phase is that there exists t such that $E_n t/(2\pi) \in \mathbb{Q}$ for $n = 2, 3, \ldots, D$. It can easily be confirmed that this condition is equivalent to that $E_n/E_1 \in \mathbb{Q}$ for $n = 2, 3, \ldots, D$. This condition is satisfied, for example, for the spectrum of harmonic oscillators.

Periodicity disappears but quasi-periodicity remains if the above condition is not satisfied, which occurs in generic interacting systems. Here we mean by quasi-periodicity that there are infinitely many recurrences during the time evolution. Mathematically speaking, the quasi-periodicity is defined by the fact that, for an arbitrary ϵ (> 0), there exists an infinite sequence t_i $(i = 1, 2, \ldots)$ such that $\| \, |\psi(t_i)\rangle - |\psi_0\rangle \, \| \leq \epsilon$. This fact is called the quantum recurrence theorem [48] and proven as follows. We begin by focusing on t_1 instead of the infinite sequence. We note that it is sufficient to prove that for an arbitrary $\delta(> 0)$ there exist t_1 and integers k_n $(n = 1, 2, \ldots, D)$ such that

$$|E_n t_1 - 2\pi k_n| \leq \delta. \tag{3.2}$$

This is because, if Eq. (3.2) holds, by putting $\delta = (\epsilon/D)^{1/2}$, we have $\| \, |\psi(t_1)\rangle - |\psi_0\rangle \, \|^2 = 2\sum_{n=1}^D [1 - \cos(E_n t_1)] \leq 2\sum_{n=1}^D \epsilon/(2D) = \epsilon$. Now, for an arbitrary $\delta(> 0)$, there exist integers $p_n(\neq 0)$ and q_n such that $|E_n/E_0 - q_n/p_n| \leq \delta/(8\pi)$ for $n = 2, 3, \ldots, D$, which follows from Dirichlet's approximation theorem [49]. It follows that $t_1 = (E_1)^{-1} 2\pi \prod_{n=2}^D p_n$ satisfies Eq. (3.2) with $k_1 = \prod_{n=2}^D p_n$ and $k_n = q_n \prod_{m(\neq n)}^D p_m$. Thus we have shown that there exists t_1 such that $\| \, |\psi(t_1)\rangle - |\psi_0\rangle \, \| \leq \epsilon$ and now it is obvious that there are $t_2, t_3, \ldots$ as well that are given, for example, by $t_i = n_i t_1$ $(i = 2, 3, \ldots)$ where $n_2 < n_3 < \ldots$ are an arbitrary sequence of ascending positive integers.

Quasi-periodicity of unitary time evolution does not preclude equilibration, that is, a phenomenon in which the system stays in a state at *almost all* times. This is because the recurrence time is extremely large and can be super-exponential of the degree of freedom in

[1] If we allow the difference only in the overall phase, we can do the parallel argument by replacing the ratios of eigenenergies E_n/E_0 in the following discussion with those of energy differences $(E_n - E_0)/(E_1 - E_0)$.

interacting many-body systems [50]. Let us provide a heuristic estimation of the recurrence time $\tau_{\rm rec}$ as follows. For a given $\epsilon(\ll 1)$, we look for $\tau_{\rm rec}$ such that $\| \, |\psi(\tau)\rangle - |\psi_0\rangle \, \| = 2\sum_{n=1}^{D}[1-\cos(E_n\tau_{\rm rec})] \leq \epsilon$. Then it is necessary that $E_n\tau_{\rm rec}$ is equal to 0 modulo 2π within the accuracy of $\epsilon^{1/2}$ for each n. Since we can expect that $\{E_n t\}_{n=1}^{D}$ spread randomly over $[0,2\pi)^D$ as t increases if the spectrum $\{E_n\}_{n=1}^{D}$ is complicated, the recurrence time $\tau_{\rm rec}$ is estimated to be proportional to $[\epsilon^{1/2}/(2\pi)]^D$. In many-body systems, the dimension D is exponentially large in the degree of freedom and thus $\tau_{\rm rec}$ is doubly exponential.

In the next section, we discuss equilibration that occurs under unitary time evolution and the effective stationary states that are seen between the recurrences.

3.2 Equilibration

Equilibration under unitary time evolution, or the existence of an effective stationary state between recurrences, has been recognized since the late 20th century [20, 51, 21] and confirmed to occur in real [37, 36, 38] and numerical [22] experiments. It is worthwhile to note that von Neumann was already aware of this in 1929 [19, 52, 53, 54] before it incurred harsh criticisms that would turn out to be invalid, and had been forgotten until quite recently. In this section, we review the theory of equilibration along these works. We note that equilibration does not refer to whether the effective stationary state is thermal, which is a separate issue discussed in the next section.

The crucial idea is that equilibration appears when we look at expectation values of few-body observables even though the quantum state itself is always changing according to Eq. (3.1). Equation (3.1) implies that the quantum state would keep changing all the time if we were able to probe all the observables including full N-body correlations. However, if we are interested only in few-body observables, different pure states can look the same in the sense that they give the same expectation values for those observables. As shown in the following, equilibration occurs in the sense that expectation values of few-body observables take the same value within small fluctuations most of the time.

Before going into details, we make a remark on the relation between equilibration and canonical typicality introduced in Chapter 2. While these notions share the idea that distinct pure states can look the same if only few-body observables are considered, the set of pure states considered are different. Whereas canonical typicality allows any linear combination $\sum_{n=1}^{D} c_n \, |E_n\rangle$ (D is the number of energy eigenstates in the microcanonical shell), unitary time evolution (3.1) constrains each weight $|c_n|^2$ to be constant. It will turn out that the

latter respecting the physically allowed states leads to richer stationary states including non-thermal states while the former always gives thermal states.

Following Short [55], let us derive equilibration in the most general manner. We allow the Hamiltonian to be degenerate and represented as

$$\hat{H} = \sum_a \epsilon_a \hat{P}_a = \sum_{n=1}^{D} E_n \left|E_n\right\rangle \left\langle E_n\right|, \tag{3.3}$$

where $\{\epsilon_a\}_a$ are the set of the distinct eigenenergies and $\hat{P}_a = \sum_{n \text{ s.t.} E_n = \epsilon_a} \left|E_n\right\rangle \left\langle E_n\right|$ is the projection operator onto the eigenspace of $\hat{H}$ with eigenenergy ϵ_a. We suppose that the initial state is represented by a density matrix $\hat{\rho}^0$, which is either pure or mixed. The density matrix at time t is given by

$$\hat{\rho}(t) = \hat{\mathcal{U}}(t)\hat{\rho}^0\hat{\mathcal{U}}(t)^\dagger = \sum_{a,b} \mathrm{e}^{-\mathrm{i}(\epsilon_a - \epsilon_b)t} \hat{P}_a \hat{\rho}^0 \hat{P}_b, \tag{3.4}$$

and the expectation value of a few-body observable $\hat{O}$ is given by

$$O(t) \equiv \mathrm{tr}\left[\hat{\rho}(t)\hat{O}\right] = \sum_{a,b} \mathrm{e}^{-\mathrm{i}(\epsilon_a - \epsilon_b)t} \mathrm{tr}\left[\hat{P}_a \hat{\rho}^0 \hat{P}_b \hat{O}\right]. \tag{3.5}$$

The central idea of equilibration is that time fluctuations of $O(t)$ around the long-time average

$$\overline{O} \equiv \lim_{T\to\infty} \int_0^T \frac{\mathrm{d}t}{T} O(t) = \sum_a \mathrm{tr}\left[\hat{P}_a \hat{\rho}^0 \hat{P}_a \hat{O}\right] = \mathrm{tr}\left[\hat{\rho}_{\mathrm{DE}} \hat{O}\right] \equiv \langle \hat{O} \rangle_{\mathrm{DE}} \tag{3.6}$$

are very small, where

$$\hat{\rho}_{\mathrm{DE}} \equiv \sum_a \hat{P}_a \hat{\rho}^0 \hat{P}_a \tag{3.7}$$

is called the diagonal ensemble because, if $\hat{H}$ is non-degenerate, it is diagonal in the energy eigenbasis. To obtain Eq. (3.6), we have used the facts that $\lim_{T\to\infty} \int_0^T \frac{\mathrm{d}t}{T} \mathrm{e}^{-\mathrm{i}(\epsilon_a - \epsilon_b)t}$ is equal to unity if $a = b$ and zero otherwise. To obtain an upper bound on the fluctuation, we make an assumption that $\hat{H}$ has non-degenerate energy gaps [51, 21, 55].

Assumption 1 (non-degenerate energy gaps)**.** If $\epsilon_a - \epsilon_b = \epsilon_c - \epsilon_d \neq 0$, then $a = c$ and $b = d$.

Indeed this assumption does not hold for noninteracting many-body systems, but is expected

to hold in generic interacting ones. The upper bound is given in the following theorem.

Theorem 2. The fluctuation of $O(t)$ is bounded from above as

$$\overline{[O-\overline{O}]^2} \equiv \lim_{T\to\infty}\int_0^T \frac{\mathrm{d}t}{T}[O(t)-\overline{O}]^2 \leq \frac{\|\hat{O}\|_{\mathrm{op}}^2}{D_{\mathrm{eff}}}, \tag{3.8}$$

where $\|\hat{O}\|_{\mathrm{op}}$ denotes the operator norm of $\hat{O}$ and the effective dimension D_{eff} is defined as

$$D_{\mathrm{eff}} \equiv \frac{1}{\sum_a \mathrm{tr}\left[\hat{P}_a\hat{\rho}^0\right]^2}. \tag{3.9}$$

Proof. First, we prove Theorem 2 when the initial state is pure and there is a state vector $|\psi_0\rangle$ satisfying $\hat{\rho}^0 = |\psi_0\rangle\langle\psi_0|$, which evolves as $|\psi(t)\rangle = \sum_a w_a^{1/2}\mathrm{e}^{-\mathrm{i}\epsilon_a t}|\epsilon_a\rangle$ with $w_a \equiv \langle\psi_0|\hat{P}_a|\psi_0\rangle\,(\geq 0)$ and $|\epsilon_a\rangle \equiv \hat{P}_a|\psi_0\rangle/w_a^{1/2}$. We note the normalization conditions $\sum_a w_a = 1$ and $\langle\epsilon_a|\epsilon_a\rangle = 1\ \forall a$. Then the fluctuation of $O(t)$ is estimated, with $\tilde{O}_{ab} \equiv \langle\epsilon_a|\hat{O}|\epsilon_b\rangle$, as

$$\begin{aligned}
\overline{[O-\overline{O}]^2} &= \sum_{\substack{a,b\\a\neq b}}\sum_{\substack{c,d\\c\neq d}} w_a^{1/2}w_b^{1/2}w_c^{1/2}w_d^{1/2}\tilde{O}_{ab}\tilde{O}^*_{cd}\lim_{T\to\infty}\int_0^T \mathrm{e}^{-\mathrm{i}[(\epsilon_a-\epsilon_b)-(\epsilon_c-\epsilon_d)]t} && (3.10)\\
&= \sum_{\substack{a,b\\a\neq b}} w_a w_b|\tilde{O}_{ab}|^2 && (3.11)\\
&\leq \sum_{a,b} w_a w_b|\tilde{O}_{ab}|^2 && (3.12)\\
&= \mathrm{tr}\left[\hat{\rho}_{\mathrm{DE}}\hat{O}\hat{\rho}_{\mathrm{DE}}\hat{O}^\dagger\right] && (3.13)\\
&\leq \sqrt{\mathrm{tr}\left[\hat{O}^\dagger\hat{O}\hat{\rho}_{\mathrm{DE}}^2\right]\mathrm{tr}\left[\hat{O}\hat{O}^\dagger\hat{\rho}_{\mathrm{DE}}^2\right]} && (3.14)\\
&\leq \|\hat{O}\|_{\mathrm{op}}^2\mathrm{tr}\left[\hat{\rho}_{\mathrm{DE}}^2\right]. && (3.15)
\end{aligned}$$

Here we have invoked Assumption 1 to obtain inequality (3.11), Schwarz' inequality to inequality (3.14), and $\mathrm{tr}[\hat{P}\hat{Q}] \leq \|\hat{P}\|_{\mathrm{op}}\mathrm{tr}[\hat{Q}]$ for positive operators $\hat{P}$ and $\hat{Q}$ to Eq. (3.15). We note that, since $\hat{\rho}_{\mathrm{DE}} = \sum_a w_a|\epsilon_a\rangle\langle\epsilon_a|$, $\mathrm{tr}\left[\hat{\rho}_{\mathrm{DE}}^2\right] = \sum_a w_a^2 = \sum_a \mathrm{tr}\left[\hat{P}_a\hat{\rho}^0\right]^2 = D_{\mathrm{eff}}^{-1}$ and thus Theorem 2 is proven for a pure initial state.

Second, we generalize the proof to a mixed state by invoking purification, which dictates that there exists a pure state $|\Psi\rangle \in \mathcal{H}\otimes\mathcal{H}$ such that $\hat{\rho}^0 = \mathrm{tr}_B[|\Psi\rangle\langle\Psi|]$, where tr_B denotes the trace over the second $\mathcal{H}$. We consider the time evolution of $|\Psi\rangle$ according to $\hat{H}' \equiv \hat{H}\otimes 1$ and the expectation value of $\hat{O}' \equiv \hat{O}\otimes 1$. We note that, since $\hat{H}$ satisfies Assumption 1, $\hat{H}'$

does as well. Thus we can apply Theorem 2 for an initial pure state, which we have proven above, to obtain $\overline{[O'-\overline{O'}]^2} \leq \|\hat{O}'\|_{\rm op}^2 {D'_{\rm eff}}^{-1}$, where ${D'_{\rm eff}}^{-1} \equiv \sum_a {\rm tr}\left[(\hat{P}_a \otimes 1)\left|\Psi\right\rangle\left\langle\Psi\right|\right]^2 = \sum_a {\rm tr}\left[\hat{P}_a\hat{\rho}^0\right]^2 = D_{\rm eff}$. We note that purification ensures $\overline{[O'-\overline{O'}]^2} = \overline{[O-\overline{O}]^2}$ and $\|\hat{O}'\|_{\rm op} = \|\hat{O}\|_{\rm op}$. Thus Theorem 2 holds also true for a mixed initial state. □

We note that the effective dimension $D_{\rm eff}$ represents the effective number of energy eigenstates involved in $\hat{\rho}^0$. Suppose that $\hat{H}$ is not degenerate and $\hat{\rho}^0$ is weighted equally over $\mathcal{N}$ energy eigenstates, then we have $D_{\rm eff} = \mathcal{N}$. If $\hat{H}$ is degenerate, $D_{\rm eff}$ represents how many eigenspaces with distinct eigenenergies are involved in $\hat{\rho}^0$. We also note that $D_{\rm eff}^{-1}$ is called the inverse participation ratio [21].

Theorem 2 implies equilibration for initial states with $D_{\rm eff}$ exponentially large in the degree of freedom (DoF) of the system because $\|\hat{O}\|_{\rm op}$ grows as a polynomial in the DoF for few-body observables (see Section 2.2.1) and thus the upper bound given in Theorem 2 is negligibly small. For these initial states, the expectation value $O(t)$ is equal to its long-time average (3.6) at almost all times. In fact, Chebyshev's inequality leads to

$$\text{Prob}\left(|O(t)-\overline{O}| > \epsilon\|\hat{O}\|_{\rm op}\right) \leq \frac{1}{\epsilon^2 D_{\rm eff}} \tag{3.16}$$

for any $\epsilon(>0)$, where Prob is defined for the uniform measure over $t \in [0,\infty)$[2]. Here we emphasize again that there remains an infinitesimal fraction of times at which $O(t)$ deviates significantly from its long-time average due to quasi-periodicity of unitary time evolution. However, Eq. (3.16) guarantees that $O(t)$ stays almost constant at the other times.

Equilibration is reached by dephasing when the initial state $\hat{\rho}^0$ is prepared to be out of equilibrium. According to Eq. (3.5), the expectation value $O(t)$ consists of a number of contributions oscillating at different frequencies. Preparing the initial state to be out of equilibrium implies that the phases of the contributions are made constructive. Then the phases become randomized in the course of time evolution, the oscillating terms cancel each other, and only non-oscillating, or diagonal, contributions remain nonvanishing most of the time.

Equilibration occurs over a wide range of systems including integrable systems as long as Assumption 1 holds and the initial state has a large effective dimension. However, the diagonal ensemble average (3.6), or the diagonal ensemble (3.7) that has all the information

[2] Strictly speaking, this probability distribution is not normalizable and one should take a finite range $[0,T]$ instead of $[0,\infty)$ to define the uniform measure, in which case a similar upper bound on the fluctuation is obtained. by using $\left|\int_0^T \frac{{\rm d}t}{T}{\rm e}^{-{\rm i}(\epsilon_a-\epsilon_b)t}\right| \leq \frac{2}{(\epsilon_a-\epsilon_b)T}$ for $a \neq b$ and Chebyshev's inequality is applicable for a sufficiently large T.

about the equilibrium state, depends on the characteristics of the system. In the next section, we discuss when and how the diagonal ensemble may be identified with the microcanonical ensemble.

3.3 Statistical-mechanical description of equilibrium states

In the previous section, we have shown, based on quantum mechanics, that an equilibrium state is represented by the diagonal ensemble (3.7) that depends on the details of the initial state $\hat{\rho}^0$. On the other hand, statistical mechanics characterises the equilibrium states with much fewer parameters. In fact, when thermalization occurs, the equilibrium state is described by the microcanonical ensemble that only refers to the total energy of the system. In this section, we review previous studies to justify the microcanonical ensemble in nonintegrable systems. Then we see that the microcanonical ensemble cannot describe systems that are integrable or exhibit localization and review approaches to characterize equilibrium states in these systems with the generalized Gibbs ensemble.

3.3.1 Eigenstate thermalization hypothesis

Equilibrium states are empirically known to be well-described by the microcanonical ensemble in nonintegrable systems where only the energy is conserved. The microcanonical ensemble is defined with two parameters, the central energy E and the energy width $\delta_{\rm mic}$, as

$$\hat{\rho}_{\rm mic}(E) \equiv W(E,\delta_{\rm mic})^{-1} \int_{E-\delta_{\rm mic}}^{E+\delta_{\rm mic}} {\rm d}E' \delta(E'-\hat{H}) \tag{3.17}$$

$$= W(E,\delta_{\rm mic})^{-1} \sum_{\substack{n \\ |E_n-E|\le\delta_{\rm mic}}} |E_n\rangle \langle E_n| , \tag{3.18}$$

where $W(E,\delta_{\rm mic})$ denotes the number of energy eigenstates in the energy window $[E-\delta_{\rm mic}, E+\delta_{\rm mic}]$ and serves as the normalization factor. It is known that the ensemble is insensitive, in the thermodynamic limit, to the choice of $\delta_{\rm mic}$ due to an exponential growth of the density of states. In finite-size systems, $\delta_{\rm mic}$ is chosen small enough compared with the range of the energy spectrum but large enough to ensure that $W(E,\delta_{\rm mic}) \gg 1$.

The eigenstate thermalization hypothesis (ETH) is regarded by many researchers as an underlying mechanism for the equivalence between the diagonal and microcanonical ensembles, which was first proposed by Deutsch [56] and Srednicki [57] based on the arguments

with the random matrix theory and the semiclassical theory, respectively. This hypothesis conjectures that the eigenstate expectation value (EEV) $\langle E_n|\hat{O}|E_n\rangle$ of a few-body observable $\hat{O}$ becomes constant over a small energy window in the thermodynamic limit. If the ETH holds true, the microcanonical ensemble is justified because $\mathrm{tr}[\hat{\rho}_{\mathrm{DE}}\hat{O}] = \mathrm{tr}[\hat{\rho}_{\mathrm{mic}}(E)\hat{O}]$ and thus the equilibrium state is indistinguishable from the microcanonical one as long as we look only at few-body observables. We note that similar scenarios have also been proposed which are known as the quantum ergodic theorem [19], the normal typicality [53], and the thermodynamic normality [54].

Purely quantum-mechanical tests of the ETH have been recently conducted using numerical full diagonalization of Hamiltonians [58, 22]. Rigol and co-workers have investigated a two-dimensional hard-core Bose-Hubbard model, which is nonintegrable [22]. For the few-body observables $\hat{n}(k_x)$, or the number of hard-core bosons with momentum k_x along the x-axis, they have calculated the expectation values of them for every energy eigenstate. They have shown that the expectation values are similar to each other within a small energy window, which is consistent with the ETH. [22] Similar tests have been done in various nonintegrable systems [59, 60, 61, 62, 63, 47, 64] and all of them seem to be consistent with the ETH except for the systems that exhibit localization [65] or that have entanglement in the energy eigenbasis [66].

Nevertheless, the ETH is still a hypothesis that has not yet been proven in any system. This is because the numerical costs grow exponentially for the full diagonalization and systems with D no more than 10^6 have been tested. For example, Rigol, Dunjko, and Olshanii [22] could test a system of 5 hard-core bosons on 21 sites that has $D = \binom{21}{5} = 20,349$. The frontier is still being pushed forward by invoking the shift-and-invert method [62] and the typicality technique [47, 64].

3.3.2 Generalized Gibbs ensemble

The microcanonical ensemble cannot describe equilibrium states in integrable systems in general even though it works for some initial conditions [67, 68, 69, 70, 64]. There are more conserved quantities in addition to the energy that constrain the time evolution. As a result, the microcanonical ensemble that uses only the total energy of the system as input parameter is no longer valid and more parameters are needed to describe the equilibrium states that are reached under the constraints.

The generalized Gibbs ensemble (GGE) has been proposed as a statistical ensemble to describe the equilibrium states in integrable systems [71, 72]. Let us denote the conserved quan-

tities by $\hat{I}_m$ ($m = 1, 2, \dots$). Then, the GGE is defined as

$$\hat{\rho}_{\rm GGE} = \frac{{\rm e}^{-\sum_m \lambda_m \hat{I}_m}}{Z} \tag{3.19}$$

with $Z = {\rm tr}[{\rm e}^{-\sum_m \lambda_m \hat{I}_m}]$. Here the parameters λ_m ($m = 1, 2, \dots$), which may be interpreted as generalized temperatures, are fixed by the conditions

$${\rm tr}\left[\hat{\rho}_{\rm GGE}\hat{I}_m\right] = {\rm tr}\left[\hat{\rho}^0\hat{I}_m\right] \quad (m = 1, 2, \dots). \tag{3.20}$$

The GGE is characterized as the ensemble $\hat{\rho}$ that maximizes the von Neumann entropy $S(\hat{\rho}) = -{\rm tr}[\hat{\rho}\ln\hat{\rho}]$ under the constraints ${\rm tr}[\hat{\rho}\hat{I}_m] = {\rm tr}[\hat{\rho}^0\hat{I}_m]$ ($m = 1, 2, \dots$) and thus the parameters λ_m ($m = 1, 2, \dots$) can also be interpreted as the Lagrange multipliers.

In the systems that can be mapped to noninteracting particles, the conserved quantities are taken as the populations in each mode. Then the GGE has been shown to describe the equilibrium states [73, 74, 75, 76, 77, 78, 79]. On the other hand, the situation is more complicated in Bethe-ansatz-solvable models. The conserved quantities are systematically obtained from generating functions and the GGE works in the XXX or XXZ models [80, 81]. However, some exceptions are known [82, 83] and it is also known that, for interaction quenches in the Lieb-Liniger model, the GGE is divergent and ill-defined [84]. Thus there remain some open questions regarding the statistical ensemble describing the equilibrium states in integrable systems.

3.3.3 Between integrable and nonintegrable systems

We discuss the effect of an integrability breaking term added on an integrable system. When the magnitude g of the integrability breaking term is perturbative, prethermalization occurs [85, 86, 87, 38]. Prethermalization is a phenomenon where the system stays in a nonthermal state before reaching the thermal state [39]. Namely, there appears a two-step relaxation: the system looks evolving as the integrable system at short times $t \ll g^{-1}$ and approaches equilibrium described by the GGE; then it approaches another equilibrium state at long times $t \gg g^{-1}$. As g increases, the prethermalized state vanishes and only an ordinary equilibration is seen.

The ETH also depends on g and numerical studies have revealed that there is a crossover where, as g increases, the ETH holds better and better and, meanwhile, the quantum chaos appears [60]. It is an open question whether, in the thermodynamic limit, there is a transition

point across which the ETH becomes to hold. This open question is related to a quantum version of the KAM theorem [88].

Chapter 4

Accuracy of Microcanonical Ensemble

In the previous chapter, we have reviewed how, in the thermodynamic limit, the microcanonical ensemble describes equilibrium states that are reached under unitary time evolution if the eigenstate thermalization hypothesis (ETH) holds true. In this chapter, we address the issue of *how accurately* the microcanonical ensemble works in small isolated quantum systems rather than *why* it does in the thermodynamic limit. First we argue that the ETH guarantees the accuracy to improve as $D^{-1/2}$ in small systems where D is the dimension of the Hilbert space. Second we conduct a numerical quench experiment and show that the accuracy improves as D^{-1}, which is much quicker than the ETH prediction. Finally, we derive the D^{-1} scaling from a statistical model that has no correlation between many-body energy eigenstates.

4.1 The ETH bound of accuracy scaling as $D^{-1/2}$

In this section, we show that the ETH guarantees that the accuracy of the microcanonical ensemble (ME) improves at least proportionally to $D^{-1/2}$ in nonintegrable systems. First we carefully argue the "thermodynamically normal" class of initial states whose energy fluctuation is sub-extensive and the ME describes the equilibrium states in the thermodynamic limit. Then we show that, in small systems, the accuracy of the ME improves as $D^{-1/2}$ for this class of initial states from the results of the finite-size-scaling analyses of the ETH.

4.1.1 Thermodynamically normal states

Let us begin by formulating the setup. We consider the same lattice quantum system as introduced in Sec. 2.2.1. We take an initial state described by a density matrix $\hat{\rho}^0$ which is either pure or mixed. The initial state evolves according to a time-independent Hamiltonian $\hat{H}$. For

simplicity, we assume that the energy spectrum of $\hat{H}$ is not degenerate and that the energy eigenstates are denoted by $\{|E_n\rangle\}_{n=1}^{D}$: $\hat{H}\,|E_n\rangle = E_n\,|E_n\rangle$ $(n = 1, 2, \dots, D)$. To guarantee equilibration to occur, we assume that the spectrum $\{E_n\}_{n=1}^{D}$ has non-degenerate energy gaps (see Assumption 1 in Sec. 3.2) and that the effective dimension is exponentially large in N:

$$D_{\rm eff} \equiv \frac{1}{\sum_{n=1}^{D}(\rho_{nn}^0)^2} = {\rm e}^{+O(N)}, \tag{4.1}$$

where $\rho_{nn}^0 \equiv \langle E_n|\hat{\rho}^0|E_n\rangle$. As shown in Chapter 3, equilibration occurs under these two assumptions.

However, not all the initial states that satisfy Eq. (4.1) are "thermodynamically normal" in the sense that the total energy of the system is not necessarily macroscopically definite. For instance, we can imagine an initial state in which ρ_{nn}^0 has two peaks around two eigenenergies that are macroscopically distinct. Indeed this state satisfies Eq. (4.1) if two peaks spread over an exponentially large number of energy eigenstates, but it is not thermodynamically normal because we encounter distinct energies every time we measure the energy of the system. Because of the same reason, even if ρ_{nn}^0 has a single peak, it is not thermodynamically normal when the energy uncertainty $\Delta E \equiv (\mathrm{tr}[\hat{\rho}^0\hat{H}^2] - \mathrm{tr}[\hat{\rho}^0\hat{H}]^2)^{1/2}$ is measurable in the thermodynamic limit.

Thus we define the initial state $\hat{\rho}^0$ to be thermodynamically normal if[1]

$$\sum_{n=1}^{D} \rho_{nn}^0\,(E_n - E)^k = o(N^k) \quad (k = 2, 3, \dots), \tag{4.2}$$

where $E \equiv \sum_{n=1}^{D} \rho_{nn}^0 E_n$ is the energy of the system and the right-hand side means that the quantity is on the order less than N^k. For $k = 2$, this condition implies that the energy uncertainty ΔE is sub-extensive. The condition for $k > 2$ implies that the higher moments of the energy distribution are convergent and the distribution does not have long tails.

For a thermodynamically normal initial state, the equilibrium state is well-described by the microcanonical ensemble if the ETH holds. First, we formulate the ETH as follows. The eigenstate expectation value (EEV) of a few-body observable $\hat{O}$ is decomposed as

$$O_n \equiv \langle E_n|\hat{O}|E_n\rangle = f_O(E_n/N) + \delta O_n, \tag{4.3}$$

[1] The right-hand side of Eq. (4.2) can be replaced by $O(N^k)$ as long as the proportionality constant is too small to be measurable.

where $f_O(x)$ is a smooth function of x. This decomposition is possible for any function $f_O(x)$ by choosing δO_n as to satisfy Eq. (4.3). The ETH dictates that there exists $f_O(x)$ such that δO_n vanishes in the thermodynamic limit. Second, we consider the expectation value of $\hat{O}$ at the equilibrium state, *i.e.*, the diagonal ensemble average of $\hat{O}$: $\langle \hat{O} \rangle_{\rm DE} = \sum_n \rho^0_{nn} O_n$ (see Eq. (3.6)). From Eq. (4.3) and the Taylor expansion of $f_O(E_n/N)$ at $E_n/N = E/N$, we have

$$\langle \hat{O} \rangle_{\rm DE} = f_O(E/N) + \sum_{k=1}^{\infty} \frac{\sum_{n=1}^{D} \rho^0_{nn} (E_n - E)^k}{N^k} \frac{f_O^{(k)}(E/N)}{k!} + \sum_{n=1}^{D} \rho^0_{nn} \delta O_n, \tag{4.4}$$

where $f^{(k)}(x)$ denotes the k-th order derivative of $f_O(x)$ and the $k = 1$ contribution in $\sum_{k=1}^{\infty}$ actually vanishes given that $\sum_{n=1}^{D} \rho^0_{nn} E_n = E$. The second term on the right-hand side of Eq. (4.4) vanishes in the thermodynamic limit if $\hat{\rho}^0$ is thermodynamically normal as defined in Eq. (4.2). The third term also vanishes in the same limit if the ETH holds true. Thus we obtain

$$\langle \hat{O} \rangle_{\rm DE} \to f_O(E/N) \quad \text{as } N \to \infty \tag{4.5}$$

Finally, we consider the microcanonical ensemble average of $\hat{O}$:

$$\langle \hat{O} \rangle_{\rm ME} \equiv \frac{1}{W(E_C, \delta_{\rm mic})} \sum_{\substack{n \\ |E_n - E_C| \le \delta_{\rm mic}}} O_n, \tag{4.6}$$

where E_C and $\delta_{\rm mic}$ are two parameters in the microcanonical ensemble representing the center and the half width of the energy window $[E_C - \delta_{\rm mic}, E_C + \delta_{\rm mic}]$, and $W(E_C, \delta_{\rm mic})$ denotes the number of energy eigenstates in the window. We take a sufficiently narrow energy window around E such that

$$\frac{1}{W(E_C, \delta_{\rm mic})} \sum_{\substack{n \\ |E_n - E_C| \le \delta_{\rm mic}}} (E_n - E)^k = o(N^k) \quad (k = 1, 2, \dots). \tag{4.7}$$

With Eq. (4.3) and the Taylor expansion of $f_O(E_n/N)$ at $E_n/N = E/N$, we have

$$\langle \hat{O} \rangle_{\rm ME} = f_O(E/N) + \sum_{k=1}^{\infty} \frac{W(E_C, \delta_{\rm mic})^{-1} \sum_{n \in \text{window}} (E_n - E)^k}{N^k} \frac{f_O^{(k)}(E/N)}{k!} + \langle \delta O \rangle_{\rm ME}, \tag{4.8}$$

where $\langle \delta O \rangle_{\rm ME} \equiv W(E_C, \delta_{\rm mic})^{-1} \sum_{n \in \text{window}} \delta O_n$. Thus, from the ETH $\delta O_n \to 0$ and Eq. (4.7),

we obtain

$$\langle \hat{O} \rangle_{\rm ME} \to f_O(E/N) \quad \text{as } N \to \infty. \tag{4.9}$$

In conclusion, if the ETH holds true, the microcanonical ensemble describes, in the thermodynamic limit, the equilibrium state that is reached starting from a thermodynamically normal initial state.

4.1.2 Accuracy of ME in small systems

Even if the ETH holds true, in small systems, the microcanonical ensemble cannot perfectly describe the equilibrium state but can do it if some error is allowed. For thermodynamically normal states, the ETH gives upper bounds on the accuracy $|\langle \hat{O} \rangle_{\rm DE} - \langle \hat{O} \rangle_{\rm ME}|$ that are obtained in the following.

In finite-size systems, the two parameters E_C and $\delta_{\rm mic}$ of the microcanonical ensemble should be optimized to minimise $|\langle \hat{O} \rangle_{\rm DE} - \langle \hat{O} \rangle_{\rm ME}|$, although they are rather arbitrarily chosen as long as we consider the thermodynamic limit. Namely, they are fixed by the following two conditions[2]:

$$\frac{1}{W(E_C, \delta_{\rm mic})} \sum_{\substack{n \\ |E_n - E_C| \le \delta_{\rm mic}}} E_n = E; \tag{4.10}$$

$$\frac{1}{W(E_C, \delta_{\rm mic})} \sum_{\substack{n \\ |E_n - E_C| \le \delta_{\rm mic}}} E_n^2 = \sum_n \rho^0_{nn} E_n^2. \tag{4.11}$$

These conditions ensure that the contributions from $k = 1$ and 2 on the right-hand side of Eqs. (4.4) and (4.8) cancel each other in $\langle \hat{O} \rangle_{\rm DE} - \langle \hat{O} \rangle_{\rm ME}$. Now we ignore the higher order derivatives since they are much smaller for thermodynamically normal states. We also ignore $\langle \delta O \rangle_{\rm ME}$ since it is the local average of δO_n and much smaller than each δO_n. Thus we obtain

$$\langle \hat{O} \rangle_{\rm DE} - \langle \hat{O} \rangle_{\rm ME} = \sum_{n=1}^{D} \rho^0_{nn} \delta O_n. \tag{4.12}$$

From Eq. (4.12), the ETH gives two upper bounds on the accuracy. The first one is given

[2] Rigorously speaking, Eqs. (4.10) and (4.11) can only be satisfied approximately because of the discreteness of the energy spectrum.

by

$$\left|\langle\hat{O}\rangle_{\mathrm{DE}} - \langle\hat{O}\rangle_{\mathrm{ME}}\right| \leq \Delta_O, \tag{4.13}$$

where Δ_O denotes the maximum deviation of δO_n from zero. The equality in Eq. (4.13) holds when ρ^0_{nn} is nonzero only for n such that $|\delta O_n| = \Delta_O$. Since $|\delta O_n|$ is maximised at a single n, the equality in Eq. (4.13) does not hold if $D_{\mathrm{eff}} \gg 1$. In that case, the accuracy is roughly bounded as

$$\left|\langle\hat{O}\rangle_{\mathrm{DE}} - \langle\hat{O}\rangle_{\mathrm{ME}}\right| \lesssim \sigma_O, \tag{4.14}$$

where σ_O is the standard deviation of δO_n. We note that Δ_O and σ_O should be calculated over a small energy window around E rather than the whole spectrum because the energy distribution ρ^0_{nn} is localized if the state is thermodynamically normal.

The ETH in the strong and weak senses respectively mean that $\Delta_O \to 0$ and $\sigma_O \to 0$ in the thermodynamic limit. The former implies that $\delta O_n \to 0$ for every energy eigenstates $|E_n\rangle$, whereas the latter does that for almost everyone. The latter allows an infinitesimal fraction of energy eigenstates that deviate the EEV from its local average.

Finite-size scaling analyses in nonintegrable spin systems have recently revealed [62, 47, **?**] that

$$\sigma_O \propto D^{-1/2} \to 0 \tag{4.15}$$

in approaching the thermodynamic limit with D the dimension of the Hilbert space. As shown in the next section, the maximum deviation Δ_O also vanishes, in nonintegrable systems, proportionally to $D^{-1/2}$. Thus, from Eq. (4.13) and (4.14), the ETH implies that the accuracy of the microcanonical ensemble improves at least proportionally to $D^{-1/2}$.

Before discussing the actual accuracy, we make a remark on the ETH in integrable systems. In those systems, the ETH breaks down in the strong sense due to the existence of the rare states that cause the EEV to deviate significantly from the local average. However, the ETH can hold in the weak sense and $\sigma_O \to 0$, in which case the decay of σ_O is only logarithmically in D [70, 89].

Table 4.1: The number N of HCBs, the number L of the lattice sites, and the dimension D of the sector (*i.e.*, the dimension of the Hilbert space) with $P = 2\pi/L$ in our numerical experiment.

N	5	6	7	8
L	15	18	21	24
D	200	1026	5537	30624

4.2 The D^{-1} scaling of accuracy

In this section, we investigate the accuracy of the microcanonical ensemble in quantum quenches in a non-integrable Bose-Hubbard model. We show that the accuracy actually improves proportionally to D^{-1}, which is much faster than the scaling of the upper bound of the accuracy given by the ETH.

4.2.1 Model

We consider a one-dimensional hard-core Bose-Hubbard model with the nearest- and next-nearest-neighbor hopping and interaction. The Hamiltonian is given by

$$\hat{H}^{(u)} = \sum_{i=1}^{L} \left[-(\hat{b}_{i+1}^{\dagger}\hat{b}_i + \hat{b}_i^{\dagger}\hat{b}_{i+1}) + u\hat{n}_i\hat{n}_{i+1} \right] + \sum_{i=1}^{L} \left[-(\hat{b}_{i+2}^{\dagger}\hat{b}_i + \hat{b}_i^{\dagger}\hat{b}_{i+2}) + \hat{n}_i\hat{n}_{i+2} \right] , \quad (4.16)$$

where $\hat{b}_i$ ($\hat{b}_i^{\dagger}$) is the annihilation (creation) operator of a hard-core boson (HCB) on site i with $[\hat{b}_i, \hat{b}_j] = [\hat{b}_i^{\dagger}, \hat{b}_j^{\dagger}] = [\hat{b}_i, \hat{b}_j^{\dagger}] = 0$ for $i \neq j$, $\hat{b}^2 = (\hat{b}^{\dagger})^2 = 0$ and $\{\hat{b}_i, \hat{b}_i^{\dagger}\} = 1$, and $\hat{n}_i \equiv \hat{b}_i^{\dagger}\hat{b}_i$. We also impose periodic boundary conditions: $b_{L+1} = b_1$ and $b_{L+2} = b_2$ in Eq. (4.16).

The nearest- and next-nearest-neighbor hopping and next-nearest-neigbhor interaction energies are, for simplicity, set to unity in Eq. (4.16). Except for $u \to \pm\infty$, this model is non-integrable and its energy level spacings obey the Wigner-Dyson statistics (see Appendix A). In the limits of $u \to \pm\infty$, the model is equivalent to the classical Ising model.

Our model (4.16) has two conserved charges, the number N of HCBs and the momentum P. In the following, we consider a sub-Hilbert space corresponding to $N = L/3$ and $P = 2\pi/L$ We note that this sector cannot be decomposed further by other symmetries. The dimensions D of this sector are listed in Table 4.1 and the energy eigenstates in the sector are denoted by $\{|E_n^{(u)}\rangle\}_{n=1}^{D}$, where the corresponding eigenenergies $\{E_n^{(u)}\}_{n=1}^{D}$ are arranged in ascending order.

4.2.2 Protocol of numerical experiment

We consider a quantum quench where the parameter u in Eq. (4.16) is suddenly changed from $u = 0$ to $u_{\rm f}$. The initial state is taken to be an energy eigenstate $|E^{(0)}_{n_0}\rangle$ of $\hat{H}^{(0)}$. The quantum quench implies that there is no change in the quantum state since the parameter u is changed instantly. The quantum state immediately after the quench is not an eigenstate of the final Hamiltonian but their superposition: $|E^{(0)}_{n_0}\rangle = \sum_n c_n |E^{(u_{\rm f})}_n\rangle$ with $c_n \equiv \langle E^{(u_{\rm f})}_n | E^{(0)}_{n_0}\rangle$. As shown in Chapter 3, if the final Hamiltonian has non-degenerate energy gaps (see Assumption 1) and the effective dimension $D_{\rm eff} \equiv 1/\sum_n |c_n|^4$ is much larger than unity, an equilibrium state appears in the course of time evolution, where the expectation value of a few-body observable $\hat{O}$ is given by the diagonal ensemble

$$\langle \hat{O} \rangle_{\rm DE} = \sum_n |c_n|^2 O_n \tag{4.17}$$

with $O_n \equiv \langle E^{(u_{\rm f})}_n | \hat{O} | E^{(u_{\rm f})}_n \rangle$. Meanwhile, we calculate the microcanonical ensemble average $\langle \hat{O} \rangle_{\rm ME}$, where the parameters are chosen to satisfy Eqs. (4.10) and (4.11), and investigate the accuracy $\langle \hat{O} \rangle_{\rm DE} - \langle \hat{O} \rangle_{\rm ME}$. We analyze two few-body observables $\hat{O}_1 \equiv \hat{n}_1 \hat{n}_2$ and $\hat{O}_2 \equiv \hat{n}_1 \hat{n}_3$ which represent the correlations between the nearest- and next-nearest-neighbors, respectively. Their operator norms are normalized to unity. We note that $\hat{O}_1$ and $\hat{O}_2$ are intensive observables because we have, for example, $\langle E^{(0)}_n | \hat{n}_1 \hat{n}_2 | E^{(0)}_n \rangle = \langle E^{(0)}_n | L^{-1} \sum_{i=1}^{L} \hat{n}_i \hat{n}_{i+1} | E^{(0)}_n \rangle$. Thus, we keep our normalization of $\hat{O}_1$ and $\hat{O}_2$ in comparing different system sizes.

The investigation of $\langle \hat{O} \rangle_{\rm DE} - \langle \hat{O} \rangle_{\rm ME}$ is done for each of the energy eigenstates of $\hat{H}^{(0)}$ whose "effective inverse temperature" lies in the interval $[0, 0.05]$, where the Boltzmann constant is set to unity. The effective inverse temperature β_n of an energy eigenstate $|E^{(0)}_n\rangle$ is defined by

$$\frac{1}{Z} \sum_{m=1}^{D} E^{(0)}_m {\rm e}^{-\beta_n E^{(0)}_m} = E^{(0)}_n, \tag{4.18}$$

where $Z \equiv \sum_{m=1}^{D} {\rm e}^{-\beta E^{(0)}_m}$. We note that β_n is uniquely determined by Eq. (4.18) because $Z^{-1} \sum_{m=1}^{D} E^{(0)}_m {\rm e}^{-\beta E^{(0)}_m}$ is a continuous and monotonically decreasing function of β and approaches $E^{(0)}_D$ and $E^{(0)}_1$ as $\beta \to -\infty$ and ∞, respectively. Table 4.2 illustrates where the energy eigenstates of $\hat{H}^{(0)}$ corresponding to the interval are in the whole spectrum. They are about 10% of all the energy eigenstates that lie just below the middle of the spectrum.

Table 4.2: For $L = 15, 18, 21$, and 24, the positions of the energy eigenstates of $\hat{H}^{(0)}$ corresponding to the interval $[0, 0.05]$ of the effective temperature are illustrated. Two symbols $n_{\rm low}$ and $n_{\rm high}$ denote the labels of the lowest and highest excited states among those having effective temperatures in the interval $[0, 0.05]$. They are about 10% of all the energy eigenstates that lie just below the middle of the spectrum.

L	15	18	21	24
$n_{\rm low}$	79	403	2140	11696
$n_{\rm low}/D$	0.40	0.39	0.39	0.38
$n_{\rm high}$	96	485	2628	14578
$n_{\rm high}/D$	0.48	0.47	0.47	0.48

4.2.3 Numerical results

The histograms of the errors $\langle\hat{O}\rangle_{\rm DE} - \langle\hat{O}\rangle_{\rm ME}$ that are obtained in the quench with $u_{\rm f} = 0.4$ of all the initial states described above are shown for $L = 18, 21$, and 24 for $\hat{O} = \hat{O}_1$ and $\hat{O}_2$, in Fig. 4.1. Figures 4.1(a) and (b) show that the distribution of $\langle\hat{O}\rangle_{\rm DE} - \langle\hat{O}\rangle_{\rm ME}$ becomes more sharply peaked around zero as the system size increases. Figure 4.1(b) also shows that the distribution of the error is well fitted by a Gaussian distribution, whose mean is much smaller than its standard deviation. Figures 4.1(c) and (d) depict those distributions for $\hat{O}_2$, which look qualitatively similar to Figs 4.1(a) and (b) although, in Fig. 4.1(d), the distribution looks slightly skewed. Here we do not go in detail about the shape of the distribution, which requires further investigation. Instead, we focus on how fast the distribution of the error $\langle\hat{O}\rangle_{\rm DE} - \langle\hat{O}\rangle_{\rm ME}$ becomes concentrated around zero as the system size increases.

We define the accuracy of the microcanonical ensemble by the root mean square (RMS) of $\langle\hat{O}\rangle_{\rm DE} - \langle\hat{O}\rangle_{\rm ME}$ that is obtained from the quenches of each initial state. In Fig. 4.2, the RMS is plotted against the system size for $\hat{O} = \hat{O}_1$ and $\hat{O}_2$. Here the error bars represent the estimation errors of the RMS calculated from the data (see Appendix B for detail). As the figure shows, the RMS decreases roughly in proportional to D^{-1}. To be more precise, with the weighted nonlinear least squares (NLLS) fittings, we have obtained the exponents of the power-law dacay as $-1.00^{+0.06}_{-0.05}$ for $\hat{O} = \hat{O}_1$ and $-1.01^{+0.05}_{-0.04}$ for $\hat{O} = \hat{O}_2$, where the 95% confidence intervals are shown (see Appendix B for detail). Thus the D^{-1} scaling of the accuracy has been confirmed.

The D^{-1} scaling has also been obtained for different quench magnitudes. Figure 4.2(b) illustrates the exponent of the scaling with the 95% confidence intervals obtained by the weighted NLLS for various $u_{\rm f}$. The data are consistent with the D^{-1} scaling for both $\hat{O}_1$ and $\hat{O}_2$ within the error bars in a wide range $0.2 \lesssim u_{\rm f} \lesssim 0.75$. In addition, the data show that

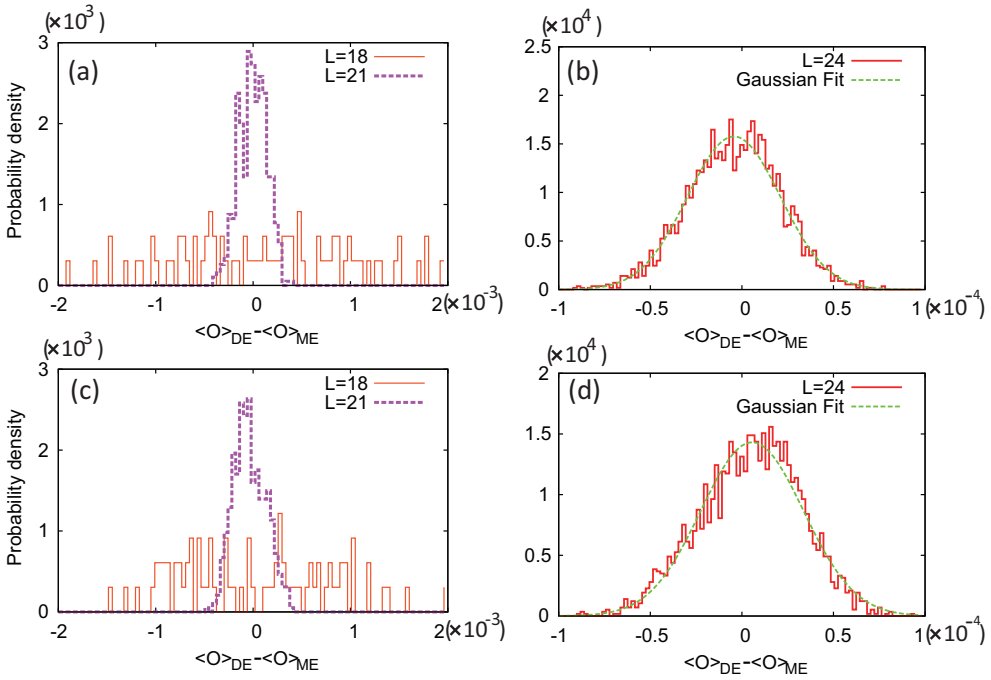

Figure 4.1: The histograms of $\langle \hat{O}_1 \rangle_{\rm DE} - \langle \hat{O}_1 \rangle_{\rm ME}$ that are obtained for the quenches of each initial state for $L = 18$ [line in (a)], $L = 21$ [dotted line in (a)], and $L = 24$ [line in (b)]. In (b), the best fit of the histogram with a Gaussian distribution is shown by the dotted curve. The panels (c) and (d) show the corresponding histograms for the other observable $\hat{O}_2$.

the exponents are clearly away from -0.5 given by the ETH (cf. Sec. 4.1).

We ignore two regions $0 \leq u_{\rm f} \lesssim 0.2$ and $u_{\rm f} \gtrsim 0.75$, where power-law decays of the accuracy look rather unclear and the weighted NLLS fittings leave large reduced chi squares. Physically speaking, the quantum states after the quench are not thermodynamically normal in these two regions. First, as for the region $0 \lesssim u_{\rm f} \lesssim 0.2$, the quench is so small that the state after the quench is close to an eigenstate of $\hat{H}^{(u_{\rm f})}$, the effective dimension is not large, and equilibration does not occur. Second, as for the region $u_{\rm f} \gtrsim 0.75$, the energy distribution $|c_n|^2$ is so broad and that the state after the quench is not thermodynamically normal. Namely, the systematic part of the EEV, or the first term on the right-hand side of Eq. (4.3), does not cancel between $\langle \hat{O} \rangle_{\rm DE}$ and $\langle \hat{O} \rangle_{\rm ME}$, and this contribution becomes dominant in larger system sizes.

The D^{-1} scaling thus obtained implies that the accuracy improves exponentially in the number N of HCBs. Let us consider a general filling factor $\nu \equiv N/L$, which is fixed to be $1/3$ in the above discussions. The dimension D is approximately given by $D \approx \binom{L}{N}/L \approx 10^{\gamma(\nu)N}$ with $\gamma(\nu) = -\nu^{-1}[\nu \log_{10} \nu + (1-\nu)\log_{10}(1-\nu)]$. We note that $\gamma(\nu)$ is a monotonically

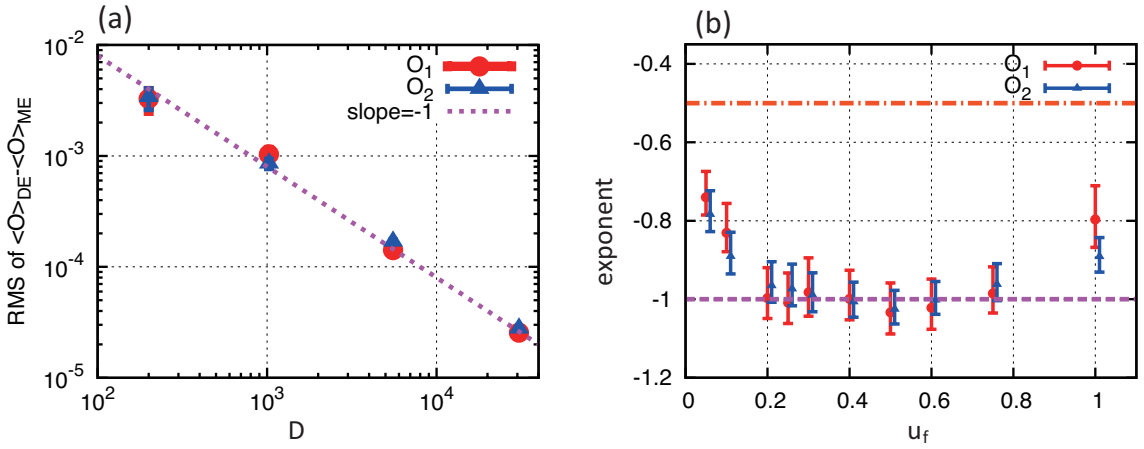

Figure 4.2: (a) For $\hat{O}_1$ (circles) and $\hat{O}_2$ (triangles), the RMS of $\langle\hat{O}\rangle_{\rm DE}-\langle\hat{O}\rangle_{\rm ME}$ obtained for each initial state is plotted against the system size shown in Table 4.1. The error bars represent the estimation error (see Appendix B). The dotted line with slope -1 is the guide to the eye. (b) For $\hat{O}_1$ (circles) and $\hat{O}_2$ (triangles), the exponent of the power-law decay of the RMS in D obtained by the weighted NLLS fit is plotted for $u_{\rm f} = 0.05, 0.1, 0.2, 0.25, 0.3, 0.4, 0.5, 0.6, 0.75,$ and 1. The data for $\hat{O}_2$ is slightly shifted to the right for visibility. The error bars represent the 95% confidence interval. The dashed-dotted line represents $-1/2$, which corresponds to the ETH prediction.

decreasing function and gives, in particular, $\gamma(1/4) = 0.9768\cdots \approx 1$. Thus the D^{-1} scaling implies that, at 1/4 filling, the accuracy $|\langle\hat{O}\rangle_{\rm DE} - \langle\hat{O}\rangle_{\rm ME}|$ improves by one order of magnitude every time we increase the number of HCBs by one.

4.2.4 Underlying mechanism for the D^{-1} scaling

Let us discuss the underlying mechanism for the D^{-1} scaling. First, we note that the ETH alone cannot explain the D^{-1} scaling. In Fig. 4.3, the two ETH bounds in Eqs. (4.13) and (4.14) are shown to be considerably larger than the accuracy that is found in our numerical experiment. Here the maximum and standard deviations of the EEV are calculated in the microcanonical window. The two bounds scale as $D^{-1/2}$ consistently with the previous studies [62, 47, **?**].

Figure 4.3 also shows that yet another indicator

$$\tilde{\sigma}_O \equiv \frac{\sigma_O}{\sqrt{D_{\rm eff}}} \tag{4.19}$$

fits the actual accuracy. We note that the $D_{\rm eff}$ is roughly proportional to D for thermodynam-

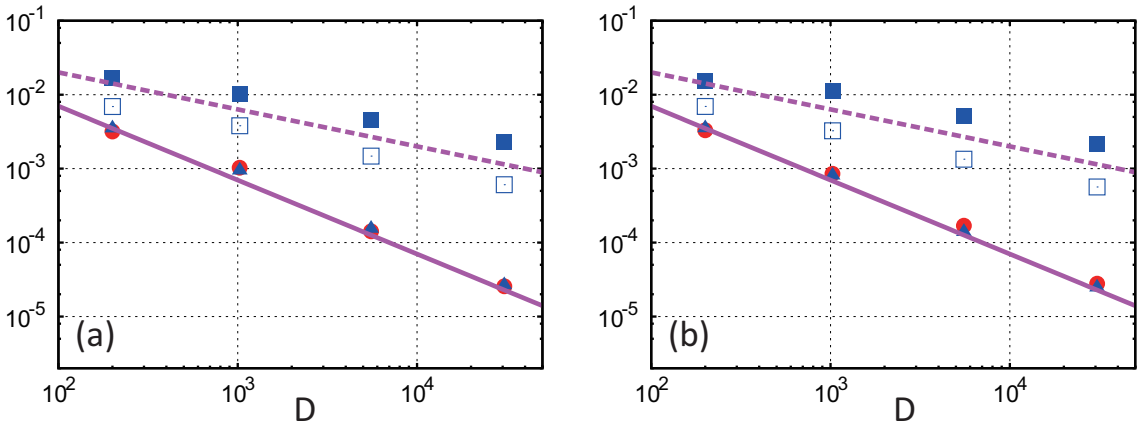

Figure 4.3: For (a) $\hat{O}_1$ and (b) $\hat{O}_2$, the accuracy of the microcanonical ensemble (circles), its bounds obtained by the strong (filled squares, Eq. (4.13)) and weak (open squares, Eq. (4.14)) ETHs, and another indicator of the no-correlation model (triangles, Eq. (4.19)) are plotted for the different system sizes shown in Table 4.1. They are calculated in the quench of $u_{\rm f} = 0.4$ and the data points represent the averages of those obtained for all the initial states. The dotted and solid lines are the guides to the eye corresponding to the slopes of $-1/2$ and -1, respectively.

ically normal states. Thus the D^{-1} scaling consists of the factor $D^{-1/2}$ coming from σ_O and the other factor $D^{-1/2}$ arising from $1/\sqrt{D_{\rm eff}}$.

Finally, we point out that we may interpret the factor $1/\sqrt{D_{\rm eff}}$ by introducing the "no-correlation model". Intuitively speaking, the no-correlation model is a statistical model in which ρ^0_{nn}'s are independent except for the two constraints: the normalization $\sum_n \rho^0_{nn}$ and the effective dimension $\sum_n (\rho^0_{nn})^2 = 1/D_{\rm eff}$. We note that, since $\hat{\rho}^0$ is thermodynamically normal, there is an effective support on which ρ^0_{nn} have significant weights. We assume that the number of energy eigenstates in the effective support is $\bar{D}_{\rm eff} (\sim 2D_{\rm eff})$ and relabel n so that $\{\rho^0_{nn}\}_{n=1}^{\bar{D}_{\rm eff}}$ are all nonzero[3]. Now we define positive random variables $\{x_n\}_{n=1}^{\bar{D}_{\rm eff}}$ that obey the same probability distribution $p(x_n)$ whose mean and variance are both unity. The no-correlation model is the statistical model with

$$\rho^0_{nn} = \frac{x_n}{\sum_{m=1}^{\bar{D}_{\rm eff}} x_m}. \tag{4.20}$$

We note that the normalization condition $\sum_{n=1}^{\bar{D}_{\rm eff}} \rho^0_{nn}$ holds for any realization and the inverse

[3] The factor 2 in $\bar{D}_{\rm eff} \sim 2D_{\rm eff}$ is chosen to make Eq. (4.24) simple. Actually, the factor can be arbitrarily chosen in deriving the D^{-1} scaling as long as the factor is independent of the system size.

of the effective dimension is typically given by

$$\left\langle \sum_{n=1}^{\bar{D}_{\rm eff}} (\rho^0_{nn})^2 \right\rangle_{\rm NCM} = \left\langle \frac{\sum_{n=1}^{\bar{D}_{\rm eff}} x_n^2}{(\sum_{m=1}^{\bar{D}_{\rm eff}} x_m)^2} \right\rangle_{\rm NCM} \tag{4.21}$$

$$\sim \frac{1}{\bar{D}_{\rm eff}^2} \left\langle \sum_{n=1}^{\bar{D}_{\rm eff}} x_n^2 \right\rangle_{\rm NCM} \tag{4.22}$$

$$= \frac{2}{\bar{D}_{\rm eff}} \tag{4.23}$$

$$\sim \frac{1}{D_{\rm eff}}, \tag{4.24}$$

where $\langle \cdots \rangle_{\rm NCM}$ denotes the average over the random variables $\{x_m\}_{m=1}^{\bar{D}_{\rm eff}}$ according to the probability distribution $p(x_1)p(x_2)\cdots p(x_{\bar{D}_{\rm eff}})$, and we have used $\sum_{m=1}^{\bar{D}_{\rm eff}} x_m \sim \bar{D}_{\rm eff}$ to obtain Eq. (4.22) since $\bar{D}_{\rm eff} \sim D_{\rm eff} \gg 1$. Now we evaluate Eq. (4.12) in terms of the no-correlation model:

$$\left\langle |\langle \hat{O} \rangle_{\rm DE} - \langle \hat{O} \rangle_{\rm ME}|^2 \right\rangle_{\rm NCM} = \sum_{n=1}^{\bar{D}_{\rm eff}} \sum_{m=1}^{\bar{D}_{\rm eff}} \left\langle \rho^0_{nn} \rho^0_{mm} \right\rangle_{\rm NCM} \delta O_n \delta O_m. \tag{4.25}$$

With $\sum_{m=1}^{\bar{D}_{\rm eff}} x_m \sim \bar{D}_{\rm eff}$, we have

$$\left\langle \rho^0_{nn} \rho^0_{mm} \right\rangle_{\rm NCM} = \begin{cases} \frac{2}{\bar{D}_{\rm eff}^2} & (m = n) \\ \frac{1}{\bar{D}_{\rm eff}^2} & (m \neq n) \end{cases} \tag{4.26}$$

since the mean and the variance of $p(x_n)$ are unity. We note that $\sum_{m=1}^{\bar{D}_{\rm eff}} \delta O_m = 0$, and obtain

$$\left\langle |\langle \hat{O} \rangle_{\rm DE} - \langle \hat{O} \rangle_{\rm ME}|^2 \right\rangle_{\rm NCM} = \frac{\sum_{n=1}^{\bar{D}_{\rm eff}} \delta O_n^2}{\bar{D}_{\rm eff}^2} = \frac{\sigma_O^2}{\bar{D}_{\rm eff}} = \tilde{\sigma}_O^2. \tag{4.27}$$

Thus we have obtained

$$|\langle \hat{O} \rangle_{\rm DE} - \langle \hat{O} \rangle_{\rm ME}| \sim \tilde{\sigma}_O, \tag{4.28}$$

which has been numerically obtained in Fig. 4.3.

The above argument implies that ρ^0_{nn}'s may be regarded as being independent of each other even though they are, in principle, determined only by the quench parameter u. The reason

behind such independence is that our model (4.16) is so complex that it is nonintegrable and exhibits quantum chaos, and thus the transition amplitudes $\langle E_n^{(u_\mathrm{f})}|E_{n_0}^{(0)}\rangle$ look independent from one n to another. In other words, the map from u_f to $\langle E_n^{(u_\mathrm{f})}|E_{n_0}^{(0)}\rangle$ for each n is so complicated that no correlation appears between ρ^0_{nn} and ρ^0_{mm} $(m \neq n)$.

4.2.5 Discussion

In conclusion, we find that the accuracy of the microcanonical ensemble scales as D^{-1} with the dimension D of the Hilbert space for quantum quenches in the hard-core Bose-Hubbard model (4.16), whereas the ETH gives upper bounds on the accuracy that scale as $D^{-1/2}$. One reason why the accuracy is actually much better than the ETH bounds is that we restrict ourselves to the thermodynamically normal initial states which have large effective dimensions D_eff that are proportional to D and small energy uncertainties. The other reason is that we cannot induce any correlations between many-body eigenstates through a quantum quench in nonintegrable systems because no fine-tuning parameters are involved in the quench, and the absence of correlations leads to the suppression factor $D_\mathrm{eff}^{-1/2}$ to the accuracy due to the law of large numbers. Due to these two reasons, the actual accuracy acquires an extra $D^{-1/2}$ scaling factor in addition to the one given by the ETH.

Finally, we speculate how the accuracy behaves even larger systems. Corresponding to the decomposition of the EEV in Eq (4.3), the error $\langle\hat{O}\rangle_\mathrm{DE} - \langle\hat{O}\rangle_\mathrm{ME}$ can also be decomposed into the systematic and fluctuation contributions. In this study, the microcanonical window has been chosen so that the systematic contribution is minimized, and, actually the fluctuation contribution has been dominant. However, considering Eqs. (4.4) and (4.8), the systematic contribution should scales as some power of the volume of the system since all the orders of the moments of the energy distribution cannot, in general, be equal to each other between the diagonal and microcanonical ensembles. Thus, there might be a system size where the systematic and fluctuation contributions become comparable and the D^{-1} scaling ends. After this point, the accuracy would vanishes algebraically in the volume. We note that, if we use the Gaussian distribution instead of the equal probability in defining the microcanonical ensemble, we may keep the D^{-1} scaling at even larger system sizes. This is because the energy distribution of quenched states tend to be Gaussian and more moments can coincide with the Gaussian version of the microcanonical ensemble with only two parameters.

Chapter 5

Entropy of Equilibrium Pure States

As discussed earlier, a single pure state can represent an equilibrium state. It is also widely accepted that isolated quantum systems such as quantum gases thermalize by themselves. Then, a natural question arises as to what is the right entropy for describing such thermal pure states. In this chapter, we discuss the microscopic definition of the thermodynamic entropy of equilibrium pure states. First, we point out that the von Neumann entropy, which is the right entropy for the description of the statistical ensembles such as the microcanonical and canonical ones, is not suitable for our purpose. Second, we introduce the diagonal entropy [42] as a generalization of the von Neumann entropy so that it is also applicable to equilibrium pure states. The rest of this chapter is devoted to show that the diagonal entropy increases upon unitary external operations consistently with the second law of thermodynamics [90]. For the sake of simplicity, the Boltzmann constant $k_{\rm B}$ is set to unity throughout this chapter.

5.1 The von Neumann entropy (vN-entropy)

In this section, we argue that the von Neumann entropy (vN-entropy) cannot represent the thermodynamic entropy of equilibrium pure states although it is very useful in quantum information theory [91] and can describe the thermodynamic entropy of the statistical ensembles.

For a given density matrix $\hat{\rho}$, the vN-entropy [92] is defined as

$$S_{\rm vN}(\hat{\rho}) \equiv -{\rm tr}(\hat{\rho}\ln\hat{\rho}). \tag{5.1}$$

This entropy is nonnegative and never exceeds $\ln D$ with D the dimension of the Hilbert space: $0 \leq S_{\rm vN} \leq \ln D$. This follows because the diagonal form, $\hat{\rho} = \sum_{i=1}^{D} p_i \left|\phi_i\right\rangle \left\langle\phi_i\right|$,

where $\{|\phi_i\rangle\}_{i=1}^D$ forms a complete orthonormal basis set and $\{p_i\}_{i=1}^D$ satisfy $\sum_i p_i = 1$ and $0 \leq p_i \leq 1$ due to positivity and the normalization of $\hat{\rho}$, leads to $S_{\rm vN}(\hat{\rho}) = -\sum_i p_i \ln p_i$ which is the Shannon entropy [93]. Thus the vN-entropy counts (in log scale) how many pure states the density matrix $\hat{\rho}$ involves. In particular, the vN-entropy vanishes only when $\hat{\rho}$ is pure, or p_i is unity for one i and zero otherwise. We note that this "counting" is performed in a basis-independent manner since the vN-entropy is invariant under an arbitrary unitary transformation $\hat{V}$: $S_{\rm vN}(\hat{\rho}) = S_{\rm vN}(\hat{V}\hat{\rho}\hat{V}^\dagger)$.

The vN-entropy has been adopted as the microscopic definition of thermodynamic entropy because it reproduces desirable properties when applied to the statistical ensembles such as the microcanonical and canonical ensembles. First, we consider the microcanonical ensemble

$$\hat{\rho}_{\rm mic}(E) \equiv W(E, \delta_{\rm mic})^{-1} \int_{E-\delta_{\rm mic}}^{E+\delta_{\rm mic}} {\rm d}E' \delta(E' - \hat{H}), \tag{5.2}$$

where $W(E, \delta_{\rm mic})$ is the number of energy eigenstates in the energy window $[E - \delta_{\rm mic}, E + \delta_{\rm mic}]$ and serves as the normalization factor: ${\rm tr}\,[\hat{\rho}_{\rm mic}(E)] = 1$. We note that $\hat{\rho}_{\rm mic}(E)$ has equal weights on every energy eigenstate in the energy window $[E-\delta_{\rm mic}, E+\delta_{\rm mic}]$ and is diagonal in the energy eigenbasis. Then the vN-entropy for the microcanonical ensemble reproduces the Boltzmann entropy

$$S_{\rm B}(\hat{\rho}_{\rm mic}(E)) = \ln W(E, \delta_{\rm mic}), \tag{5.3}$$

and thus can be considered as a thermodynamic entropy. Second, we consider the canonical ensemble

$$\hat{\rho}_{\rm can}(\beta) = \frac{{\rm e}^{-\beta\hat{H}}}{Z}, \tag{5.4}$$

where β is the inverse temperature and $Z \equiv {\rm tr}({\rm e}^{-\beta\hat{H}})$ is the partition function. Again, this ensemble is diagonal in the energy eigenbasis and leads to

$$F = E - TS_{\rm vN}(\rho_{\rm can}(\beta)), \tag{5.5}$$

where $F \equiv -\beta^{-1} \ln Z$ and $E \equiv {\rm tr}[\hat{\rho}_{\rm can}(\beta)\hat{H}]$ denote the free and internal energies. Thus the vN-entropy can be considered as the thermodynamic entropy when applied to the canonical ensemble. We note that the similar argument can be applied to the grand canonical ensemble and the generalized Gibbs ensemble [72]. Thus the vN-entropy is consistent with thermody-

namics when applied to the statistical ensembles.

However, the vN-entropy cannot represent the thermodynamic entropy of pure states at equilibrium because, as noted above, it vanishes for any pure states regardless of the total energy, or equivalently the temperature, of the state. To put it differently, the vN-entropy is defined independently of the basis, so if we choose an appropriate basis set such that the pure state representing $\hat{\rho}$ is a member, it vanishes; however, if we expand $\hat{\rho}$ in terms of the eigenenergy basis, there is, in general, more than one non-vanishing diagonal element that the thermodynamic entropy counts in, for example, Eq. (5.3).

Another problem of the vN-entropy is that it is inconsistent with the second law of thermodynamics when we consider external operations within the unitary time evolution. Since the vN-entropy is, as noted above, invariant under any unitary transformation, it stays constant during any unitary external operation such as a change in an external magnetic field. This contradicts the second law of thermodynamics, which dictates that the entropy increase unless the external operation is adiabatic or done infinitely slowly. This is another problem of the basis-independence of the vN-entropy.

Therefore, to quantify the thermodynamic entropy of equilibrium pure states consistently with thermodynamics, we need to generalize the vN-entropy so that it is also applicable to equilibrium pure states. The key idea is to respect the energy eigenbasis and we arrive at the concept of the diagonal entropy introduced in the next section.

5.2 The diagonal entropy (d-entopy)

We adopt the diagonal entropy (d-entropy) [42] as a generalization of the vN-entropy such that it is also applicable to equilibrium pure states. For a density matrix $\hat{\rho}$, the d-entropy is defined as

$$S(\hat{\rho}) = -\sum_n \rho_{nn} \ln \rho_{nn}, \tag{5.6}$$

where ρ_{nn} is the diagonal elements of $\hat{\rho}$ in the energy eigenbasis. Thus the d-entropy depends not only on the quantum state but also on the Hamiltonian of the system of interest. As stated in Section 5.1, Eq. (5.6) effectively counts the number of energy eigenstates involved in $\hat{\rho}$.

The d-entropy coincides with the vN-entropy for the density matrix $\hat{\rho}$ that is diagonal in the energy eigenbasis as it directly follows from Eqs. (5.1) and (5.6). In particular, since the microcanonical and canonical ensembles are diagonal in the energy eigenbasis, the d-

entropy reproduces Eqs. (5.3) and (5.5) as does the vN-entropy. In this sense, the d-entropy is a generalization of the vN-entropy.

Unlike the vN-entropy, the d-entropy can be nonzero for pure states if more than one energy eigenstate is superposed. Considering thermal pure quantum (TPQ) states reviewed in Chapter 2, we obtain the Boltzmann entropy from the d-entropy whereas the vN-entropy always vanishes for such states. It is because the TPQ states typically consist of all the energy eigenstate in an energy window $[E-\delta_{\rm mic}, E+\delta_{\rm mic}]$ and the d-entropy reduces to the logarithm of the number of energy eigenstates in the window. Thus the d-entropy gives results consistent with the vN-entropy for thermodynamic ensembles and provides the nonvanishing entropy for TPQ states.

As for the second law of thermodynamics, the d-entropy has been shown [42] to increase when an arbitrary unitary operation $\hat{V}$ is performed on a state represented by the density matrix $\hat{\rho}$ diagonal in the energy eigenbasis. This result is obtained as follows. Let us act an arbitrary unitary operator $\hat{V}$ on a density matrix $\hat{\rho}$, which is diagonal in the energy eigenbasis. We denote by ρ_{nn} the diagonal elements; then the d-entropy S of this state is given by Eq. (5.6). Now we consider the diagonal elements ρ'_{nn} of the state after the operation in energy eigenbasis, where the Hamiltonian may or may not be the same Hamiltonian before the operation. Then there exists a unitary matrix U_{nm} such that $\rho'_{nn} = \sum_m |U_{nm}|^2 \rho_{mm}$ and the d-entropy after the operation is given by $S' = -\sum_n \rho'_{nn} \ln \rho'_{nn}$. Due to the convexity of the function $f(x) = -x \ln x$, we obtain $S' \geq -\sum_n \sum_m |U_{nm}|^2 \rho_{mm} \ln \rho_{mm} = S$ and the d-entropy thus never decreases upon any unitary operation if the state is diagonal.

Indeed this is consistent with thermodynamics, but not fully satisfactory because it can be applied only once because, if the initial state of the operation is diagonal in the energy eigenbasis, the final state is not in general diagonal in the energy eigenbasis. When we have a sequence of equilibrium pure states that are obtained by unitary external operations, the d-entropy should increase upon each operation to be consistent with the second law of thermodynamics. To solve this problem, it is necessary to relax the restriction of the states on which an external operation is performed. In the following section, we show that the d-entropy increases upon unitary external operations performed on equilibrium states including pure states.

We emphasize that this is not a minor generalization but involves deeper insights. Namely, the asymmetry between the increase and decrease emerges in the d-entropy, whereas the entire time evolution including external operations is unitary and thus reversible. The above argument attributes the asymmetry in the specialty of the states on which an external op-

eration is performed similarly to other works that derives the irreversibility within unitary evolution [94, 95]. In contrast, we geometrically illustrate in Section 5.4 that the asymmetry emerges from the fact that the quantum states allowed in unitary evolution is restricted to a subspace rather than the entire Hilbert space.

5.3 The d-entropy increase upon unitary external operations

In this section, we discuss the d-entropy change upon an arbitrary unitary external operation performed on pure/mixed states at equilibrium. The key in our formulation is that we focus on the timing at which a given operation $\hat{V}$ is performed. We show that the d-entropy increases not only on average but also at typical such timings.

5.3.1 Setup

We assume the dimension D of the Hilbert space is either finite or countably infinite. The quantum state at time $t = 0$ is represented by a density matrix $\hat{\rho}^0$, which is either pure or mixed. The quantum state at time t is given by $\hat{\rho}(t) = \hat{\mathcal{U}}(t)\hat{\rho}^0\hat{\mathcal{U}}(t)^\dagger$, where the time evolution operator is given by $\hat{\mathcal{U}}(t) = \mathrm{e}^{-\mathrm{i}\hat{H}t/\hbar}$, with $\hat{H}$ being a time-independent Hamiltonian. We denote by $\{|E_n\rangle\}_{n=1}^D$ the eigenstates of $\hat{H}$ with its spectrum $\{E_n\}_{n=1}^D$: $\hat{H}\,|E_n\rangle = E_n\,|E_n\rangle$ $(n = 1, 2, \ldots, D)$. We assume that $\hat{H}$ is non-degenerate so that the d-entropy of $\hat{\rho}^0$ (see Eq. (5.6)) is uniquely defined by

$$S_0 = -\sum_n \rho^0_{nn} \ln \rho^0_{nn}, \tag{5.7}$$

where $\rho^0_{nn} \equiv \langle E_n|\hat{\rho}^0|E_n\rangle$. We note that the d-entropy never changes during the time evolution $\hat{\mathcal{U}}(t)$ since no transitions occur between the energy eigenstates.

We assume that the spectrum $\{E_n\}_{n=1}^D$ has non-degenerate energy gaps.

Assumption 2 (Non-degenerate energy gaps)**.** $E_k - E_l = E_m - E_n$ implies $k = m$ and $l = n$.

To ensure equilibration to occur in the time evolution, we need to also assume that the effective dimension of $\hat{\rho}^0$ is exponentially large as explained in Chapter 3. Nevertheless, we do not for now since Theorems 3 and 4 can be proven without it. We will return to this assumption after proving them.

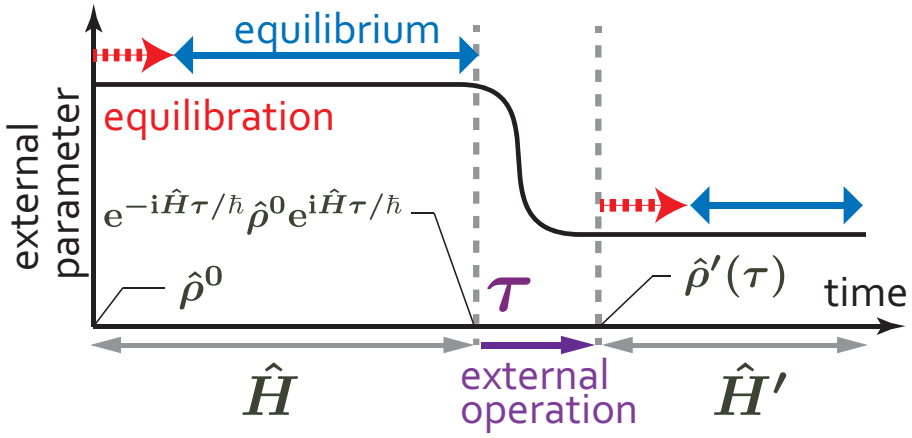

Figure 5.1: Schematic figure of our setup. The initial state $\hat{\rho}^0$ evolves as $\hat{\mathcal{U}}(t)\hat{\rho}^0\hat{\mathcal{U}}(t)^\dagger$ from $t = 0$ to τ, during which the stationary state is achieved. At time $t = \tau$, an unitary operation $\hat{V}$ is performed by changing an external parameter in the Hamiltonian. After the operation, the system evolves according to $\hat{H}'$ and approaches to another stationary state.

An external operation represented by an arbitrary unitary operator $\hat{V}$ is performed at $t = \tau$. In the case, for example, that the Hamiltonian is varied from $t = \tau$ to $t = \tau + \Delta\tau$ through a parameter like a magnetic field, the operator $\hat{V}$ is given by $\hat{V} = \mathbb{T}\exp\left[-\frac{\mathrm{i}}{\hbar}\int_\tau^{\tau+\Delta\tau}\hat{H}(t')\mathrm{d}t'\right]$, where $\mathbb{T}$ denotes the time-ordering product. In our setup, we fix the unitary operation $\hat{V}$ and regard τ as a variable.

Immediately after the external operation, the density matrix is given by

$$\hat{\rho}'(\tau) = \hat{V}\hat{\mathcal{U}}(\tau)\hat{\rho}^0\hat{\mathcal{U}}(\tau)^\dagger\hat{V}^\dagger. \tag{5.8}$$

Here we note that this is not necessarily the state at time $t = \tau$ because the operation may take a nonzero time (see Fig. 5.1). We do not specify the time at which the operation $\hat{V}$ is finished since it is arbitrary. We denote by $\hat{H}'$ the Hamiltonian immediately after the operation which is time independent after the operation. We denote by $\{|E'_n\rangle\}_{n=1}^D$ the eigenstates of $\hat{H}'$ with its spectrum $\{E'_n\}_{n=1}^D$: $\hat{H}'|E'_n\rangle = E'_n|E'_n\rangle$ $(n = 1, 2, \ldots, D)$. We assume that the spectrum is non-degenerate to make the d-entropy after the operation well-defined and uniquely given by

$$S'(\tau) = -\sum_n \rho'_{nn}(\tau)\ln\rho'_{nn}(\tau), \tag{5.9}$$

where $\rho'_{nn}(\tau) \equiv \langle E'_n|\hat{\rho}'(\tau)|E'_n\rangle$. This d-entropy does not vary after the operation since the Hamiltonian $\hat{H}'$ is independent of time.

The fact that the d-entropy never changes during time evolution according to a time independent Hamiltonian implies that the d-entropy does not represent the entropy of states out of equilibrium because such an entropy, if exists, is believed to increase as the system approaches a stationary state. Instead, the d-entropy can be interpreted to represent the one for the stationary state that is realized as a result of the time evolution according to a given time-independent Hamiltonian.

5.3.2 The d-entropy after the external operation

The diagonal initial state

Before working on our initial state involving a pure state, we review the previous study that has shown the d-entropy increases when $\hat{\rho}^0$ is diagonal in the energy eigenbasis. We take as an initial state the diagonal ensemble

$$\hat{\rho}^0_{\rm DE} \equiv \sum_n \rho^0_{nn} \left|E_n\right\rangle \left\langle E_n\right|, \tag{5.10}$$

which has the same diagonal elements as our initial state $\hat{\rho}^0$ and thus the same d-entropy S_0. Since $\hat{\rho}^0_{\rm DE}$ is diagonal, it is time-independent under the time evolution $\hat{\mathcal{U}}(t)$ and the d-entropy after the operation does not depend on τ and is given by

$$S'_{\rm DE} = -\sum_n \mu_n \ln \mu_n, \tag{5.11}$$

where $\mu_n \equiv \langle E'_n|\hat{V}\hat{\rho}^0_{\rm DE}\hat{V}^\dagger|E'_n\rangle = \sum_m |U_{nm}|^2\rho^0_{mm}$ with $U_{nm} \equiv \langle E'_n|\hat{V}|E_m\rangle$. Then it follows that

$$S_0 \le S'_{\rm DE} \tag{5.12}$$

for any external operation $\hat{V}$. In fact, since $f(x) = -x\ln x$ is convex up, we obtain $S' \ge \sum_n \sum_m |U_{nm}|^2(-\rho^0_{mm}\ln\rho^0_{mm}) = S_0$.

We emphasize again that this argument of the d-entropy increase cannot be applied repeatedly in a sequence of external operations. This is because the final state $\hat{\rho}'_{\rm DE}$ is no longer diagonal in the eigenbasis of $\hat{H}'$ in general even though it can reach another equilibrium state in the unitary time evolution. Our motivation is to relax the condition of the initial state so

that it can be applied repeatedly.

The general initial state

Returning to the original problem, we consider the long-time average of $S'(\tau)$ when τ is uniformly distributed over $[0, \infty)$. The following theorem gives bounds on the long-time average (see Appendix C for the proof).

Theorem 3. We have

$$0 \leq S'_{\mathrm{DE}} - \overline{S'(\tau)} < 1, \tag{5.13}$$

where $\overline{F(\tau)} \equiv \lim_{T\to\infty} \int_0^T \frac{\mathrm{d}\tau}{T} F(\tau)$.

This theorem, together with Eq. (5.12), implies

$$S_0 - 1 < \overline{S'(\tau)}, \tag{5.14}$$

which implies the second law of thermodynamics when the sub-extensive correction 1 can be ignored such as in the thermodynamic limit.

Theorem 3 estimates the noncommutativity between taking the d-entropy and the long-time average. While we are considering the long-time average of the d-entropy, we can also consider the d-entropy of the long-time averaged state. These are given by $\overline{S'(\tau)}$ and $S'_{\mathbf{DE}}$, respectively, and different from each other, in general, since the off-diagonal elements of the density matrix in the energy eigenbasis survive in the unitary time evolution. Theorem 3 dictates that the difference is less than unity, which is sub-extensive.

We note that a stronger inequality $S_0 \leq \overline{S'(\tau)}$ does not hold in general. An exception to this inequality occurs when $\hat{\rho}^0 = |\phi\rangle\langle\phi|$ with $|\phi\rangle = D^{-1}\sum_n |E_n\rangle$ for a finite D. Then, we have $S_0 = S'_{\mathrm{DE}} = \ln D$, but $\overline{S'(\tau)} < \ln D$ in general. Hoever, Theorem 3 ensures the decrease of the d-entropy is no greater than unity, which is sub-extensive.

The second theorem gives a lower bound on the probability of τ at which $S'(\tau)$ is greater than a certain value (see Appendix C for the proof).

Theorem 4. We have

$$\mathrm{Prob}\left[S_0 - S_0^{2/3} < S'(\tau)\right] \geq 1 - \frac{2S'_{\mathrm{DE}}}{S_0^{4/3}} - \frac{R}{S_0^{4/3}}, \tag{5.15}$$

where $R \equiv \sum_{m,n} \nu_{mn} \ln \mu_m \ln \mu_n$ with $\nu_{mn} \equiv \sum_{\substack{k,l \\ k \neq l}} U_{mk} U_{nl}^* U_{nk}^* U_{ml} |\rho_{kl}^0|^2$, and Prob is defined for τ that uniformly distributes over $[0, \infty)$.

As discussed later, when the d-entropy is extensive, this theorem implies that the d-entropy increases for almost all τ in the thermodynamic limit.

5.3.3 Extensivity and increase of the d-entropy in lattice systems

In this section, we apply Theorems 3 and 4 to lattice systems to discuss the extensivity and the increase of the d-entropy. We assume the total Hilbert space of the lattice system is a direct product of N identical Hilbert spaces with dimension $d\,(\geq 2)$. Namely, N denotes the number of lattice points and $D = d^N$.

We assume that the effective dimension of the initial state $\hat{\rho}^0$ is exponentially large.

Assumption 3.

$$D_{\text{eff}} \equiv \frac{1}{\sum_n (\rho_{nn}^0)^2} = \mathrm{e}^{+O(N)}. \tag{5.16}$$

This assumption ensures not only that equilibration occurs in time evolution $\hat{\mathcal{U}}(t)$ but also that S_0 is extensive, or proportional to N. In fact, the convexity leads to $S_0 \geq -\ln[\sum_n \rho_{nn}^0)^2] = \ln D_{\text{eff}} = O(N)$ and we have an upper bound $S_0 \leq \ln D = N \ln d$. For the same reason, S'_{DE} is also extensive.

Here and henceforth, by $\lesssim$ and $\sim$ we mean $\leq$ and $=$, respectively, with sub-leading terms in N ignored. For example, Eq. (5.14) implies $S_0 \lesssim \overline{S'(\tau)}$ since S_0 is extensive and 1 is not. Besides, Theorem 4 implies $\text{Prob}[S_0 \lesssim S'(\tau)] \sim 1$ since $R = \mathrm{e}^{-O(N)}$ as shown in Appendix C. Thus we obtain the following two corollaries.

Corollary 1.

$$S_0 \lesssim \overline{S'(\tau)}. \tag{5.17}$$

Corollary 2.

$$\text{Prob}[S_0 \lesssim S'(\tau)] \sim 1. \tag{5.18}$$

Corollaries 1 and 2 are consistent with the second law of thermodynamics from the viewpoint of the fluctuation theorem. Since we have assumed Assumptions 2 and 3, equilibration

occurs in the time evolution $\hat{\mathcal{U}}(t)$ and different states in the equilibrium ensemble are expected to realize at each $t = \tau$ sampled uniformly. The fluctuation theorem dictates that there exist some probability in sampling, from the equilibrium ensemble, states in which the entropy decreases but the entropy never decreases on average over the samplings. This is consistent with Corollary 1. The fluctuation theorem also dictates that the probability at which the entropy decreases becomes vanishingly small in the thermodynamic limit, which is consistent with Corollary 2.

Our argument can be applicable to another external operation performed on the final state in our setup if $\hat{H}'$ has non-degenerate energy gaps (Assumption 2) and the final state has an exponentially large effective dimension (Assumption 3). Actually, the exponentially large effective dimension is guaranteed by the increase of the d-entropy in our setup. Thus, we reach the following conclusion: provided that the system has nondegenerate energy gaps and starts with an initial state of an exponentially large effective dimension, the d-entropy increases for a sequence of external operations during which the Hamiltonian changes.

5.3.4 The reverse process

Our argument of the d-entropy increase is also applicable to the reverse process shown in Fig. 5.2 if Assumptions 2 and 3 are satisfied. We fix $\tau = \tau_1$ and define the final state of the forward process by $\hat{\rho}^f_{\tau_2} = \mathrm{e}^{-\mathrm{i}\hat{H}'\tau_2/\hbar}\hat{\rho}'(\tau_1)\mathrm{e}^{\mathrm{i}\hat{H}'\tau_2/\hbar}$, where τ_2 is the duration of time evolution with $\hat{H}'$ after the external operation is finished. Suppose that the d-entropy increases in this process: $S_0 < S'(\tau_1)$. We define the reverse process such that the initial state is $\hat{\rho}^f_{\tau_2}$ at $\tilde{t} = 0$ and evolves in time according to $-\hat{H}'$, and assume that an external operation $\hat{V}^\dagger$ is performed at $\tilde{t} = \tilde{\tau}$. To make Corollary 2 applicable to the reverse process, we assume that $\hat{H}'$ has non-degenerate energy gaps (see Assumption 2 and the effective dimension of $\hat{\rho}^f_{\tau_2}$ is exponentially large (see Assumption 3).

For a special choice of $\tilde{\tau} = \tau_2$, the d-entropy is decreased by the operation in the reverse process. This is because, in the reverse process, the d-entropies before and after the operation are equal to $S'(\tau_1)$ and S_0, respectively, that have been supposed to satisfy $S'(\tau_1) > S_0$. In this case, the quantum state retraces exactly the same path of the forward process in the opposite direction of time.

The existence of the operation timing at which the d-entropy decreases does not contradict Corollary 2, which states that the d-entropy increases for *almost* all timings of the external operation rather than for all timings. Corollary 2 implies that, to decrease the d-entropy, we must do fine-tuning on the timing of the operation based on a priori knowledge about, e.g.,

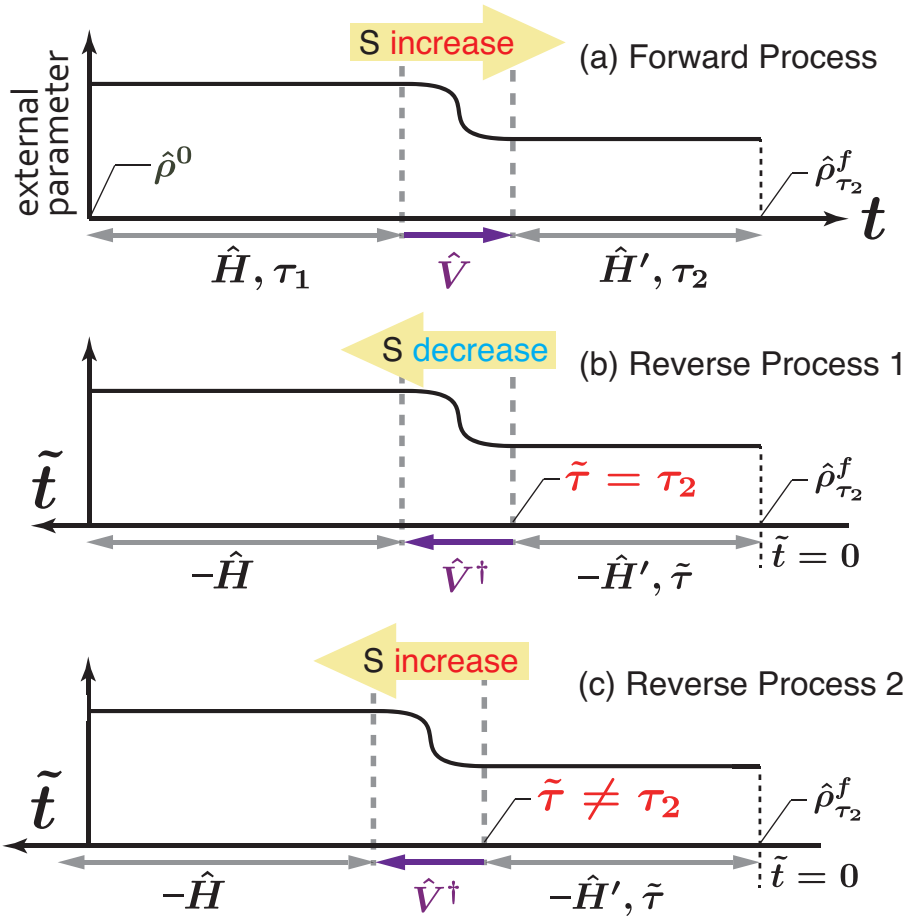

Figure 5.2: Schematic figure of the forward and reverse processes. (a) We suppose that the d-entropy increases for $\tau = \tau_1$. (b) The d-entropy can decrease for a special choice of $\tilde{\tau} = \tau_2$ in the reverse process. This follows from the assumption that the d-entropy increases in the forward process. (c) The d-entropy increases for typical $\tilde{\tau}$ if $\tilde{\tau} \neq \tau_2$. This follows from Corollary 2, which does not contradict (b) since it allows the operation timings of zero measure at which the d-entropy decreases.

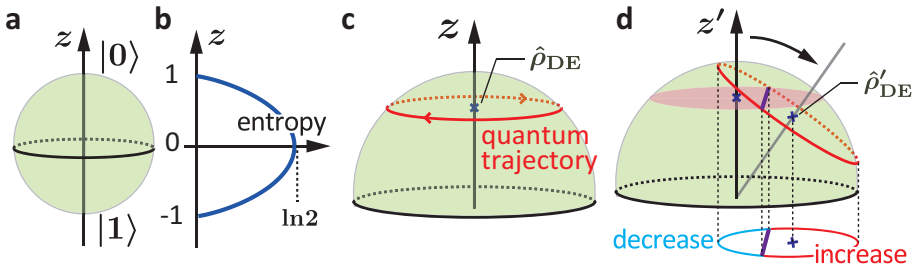

Figure 5.3: The asymmetry between the d-entropy increase and decrease for a qubit system. (a) The Bloch sphere, where the $z = \pm 1$ correspond to $|0\rangle$ and $|1\rangle$ that are the eigenstates of $\hat{H}$. (b) The d-entropy depends only on the z-coordinate and monotonically increases from the poles to the equator. (c) Under time evolution with $\hat{H}$ the state traces a circle perpendicular to the z-axis that we call a quantum trajectory whose projection onto the z-axis is corresponding to $\hat{\rho}_{\rm DE}$ [Eq. (5.11)]. (d) An external operation together with changing the basis to the eigenstates of $\hat{H}'$ rotates the Bloch sphere and thus tilts the quantum trajectory. Then the center of the quantum trajectory approaches the equator, which implies Eq. (5.12). Meanwhile, more than half of the quantum states on the quantum trajectory approach the equator, which means that the d-entropy increases for more than 50%.

the forward process. This is how we obtain the d-entropy increase for both the forward and its reverse processes.

5.4 Geometrical interpretations of asymmetry in d-entropy increase/decrease

In this section, we geometrically interpret how the asymmetry between the increase and decrease arises within unitary time evolution, which is reversible. We consider one qubit, the two-dimensional Hilbert space, to demonstrate that it originates from the fact that the quantum states allowed under unitary evolution are restricted.

A qubit is defined on a two-dimensional Hilbert space: $D = 2$. An arbitrary density matrix $\hat{\rho}$ representing the state of the qubit corresponds to a point on or inside the Bloch sphere (see Fig. 5.3). The x-, y-, and z-components of $\hat{\rho}$ are defined as $x = \mathrm{tr}(\hat{\rho}\hat{\sigma}_x)$, $y = \mathrm{tr}(\hat{\rho}\hat{\sigma}_y)$, and $z = \mathrm{tr}(\hat{\rho}\hat{\sigma}_z)$, where $\hat{\sigma}_x, \hat{\sigma}_y$, and $\hat{\sigma}_z$ are the Pauli matrices. We take the z-direction as the eigenbasis of the Hamiltonian $\hat{H}$: $[\hat{H}, \hat{\sigma}_z] = 0$.

The d-entropy of $\hat{\rho}$ in our convention is given by

$$S(\hat{\rho}) = -\left(\frac{1-z}{2}\right)\ln\left(\frac{1-z}{2}\right) - \left(\frac{1+z}{2}\right)\ln\left(\frac{1+z}{2}\right). \tag{5.19}$$

As illustrated in Fig. 5.3b, the d-entropy is even under changing the sign of z and monotonically increasing from $z = \pm 1$ to $z = 0$.

An arbitrary initial state $\hat{\rho}^0$ traces a circle, the quantum trajectory, which is perpendicular to the z-axis under unitary evolution according to $\hat{H}$ as depicted in Fig. 5.3c. The projection of the trajectory onto the z-axis corresponds to the diagonal ensemble (5.10).

At time $t = \tau$, we perform a unitary external operation $\hat{V}$, during which the Hamiltonian $\hat{H}$ changes to $\hat{H}'$. Figure 5.3 shows the Bloch sphere where the z'-axis are taken so that $z' = \pm 1$ correspond to two eigenstates of $\hat{H}'$. The external operation and the change of basis act on the Bloch sphere as a rotation, which tilts the quantum trajectory. In this rotation, if the initial state is away from the equator, the center of the trajectory approaches the equator, which means Eq. (5.12). This implies that the d-entropy is increased for more than half of the states on the trajectory. Hence follows the asymmetry between the d-entropy increase and decrease. Namely, the asymmetry arises from the fact that the quantum trajectory does not cover the entire Hilbert space but it is restricted to its subspace. Corollary 2 dictates that this asymmetry is enhanced as the system size increases.

We note that, if the initial state is on the equator, the d-entropy decreases most likely. However, this does not contradict Corollary 2 in larger dimensions because Theorem 3 ensures that the decrease is only sub-extensive. Thus, once the equator, or the infinite temperature, is reached, the d-entropy is actually saturated.

5.5 The Universal Sub-Extensive Correction

Here we discuss sub-extensive contributions in the d-entropy whereas we have been considering the leading terms in the system size. We conjecture a more stringent inequality than that given in Theorem 3.

Conjecture.

$$0 \leq S'_{\mathrm{DE}} - \overline{S'(\tau)} \leq 1 - \gamma \tag{5.20}$$

with $\gamma = 0.5772\ldots$ the Euler's constant, where the equality on the right holds if the initial state is pure and the external operation induces numerous transitions between the energy eigenstates.

This conjecture is obtained as follows. We have $\overline{\rho'_{nn}(\tau)} = \mu_n$ and $\overline{[\rho'_{nn}(\tau)]^2} = 2\mu_n^2$. Thus we expect $\overline{[\rho'_{nn}(\tau)]^{1+\epsilon}} \leq \Gamma(2+\epsilon)\mu_n^{1+\epsilon}$ for $0 \leq \epsilon \leq 1$, where $\Gamma(x)$ is the Gamma function. We have $\overline{\rho'_{nn}(\tau)\ln\rho'_{nn}(\tau)} \leq \mu_n \ln \mu_n + \Gamma'(2)\mu_n$ by taking the limit of $\epsilon \to 0$. By taking the sum over n, we obtain $S'_{\rm DE} - \overline{S'(\tau)} \leq 1 - \gamma$, where we have used $\Gamma'(2) = 1 - \gamma$. We derive the equality condition by invoking the replica trick in Appendix C.

Now we provide numerical evidences for our conjecture. We consider five hard-core bosons (HCBs) on 20 sites that are arranged in a 4×5 rectangular shape. We assign coordinates (x_i, y_i) for each site, where i ($i = 1, 2, \ldots, 20$) labels the sites and $x_i = 1, 2, 3, 4, 5$ and $y_i = 1, 2, 3, 4$. The Hamiltonian $\hat{H}(g)$ is given by

$$\hat{H}(g) = -J \sum_{\langle i,j \rangle} (b_i^\dagger b_j + b_j^\dagger b_i) + g \sum_i y_i b_i^\dagger b_i, \tag{5.21}$$

where b_i and $b_i^\dagger$ denote the annihilation and creation operators of HCB on site i and $\sum_{\langle i,j \rangle}$ denotes the sum over pairs of adjacent sites. The first and second terms on the right-hand side of Eq. (5.21) represent the hopping of HCBs and a linear potential along the y-axis. The dimension D of the Hilbert space is given by $D = \binom{20}{5} = 15,504$ from the hard-core condition that prohibits more than one HCB from occupying a single site.

The initial state is taken as the 1000th eigenstate of $\hat{H}(g = 0)$ in an ascending order of eigenenergy and evolves until $t = \tau$ according to $\hat{H}(g)$ where $g(> 0)$ is the control parameter in our numerics. At time $t = \tau$ we perform an external operation, which is a quantum quench, or a sudden switch-off of g to 0. We plot $S'_{\rm DE} - \overline{S'(\tau)}$ for various g in Fig. 5.4, where $\overline{S'(\tau)}$ is calculated from $S'(\tau)$ in the time interval $[500, 1000]\hbar/J$. The error bars show the standard deviations of $S'(\tau)$ in the same interval. The reason why we have taken the 1000th eigenstate is that more energy eigenstates are involved after the quench than the ground state, and they suppress the standard deviations within the small Hilbert space dimension that are numerically addressable.

Figure 5.4 shows that all the data points are below the bound $1-\gamma$, which is consistent with Conjecture 5.5. Besides, it also shows that $S'_{\rm DE} - \overline{S'(\tau)} = 1 - \gamma$ independently of the quench magnitude for large quenches $g/J \gtrsim 0.25$. Since our initial state is pure, this is consistent with the equality condition dictated in Conjecture 5.5.

The universal constant $1 - \gamma$ can be used to judge whether or not the initial state is pure if

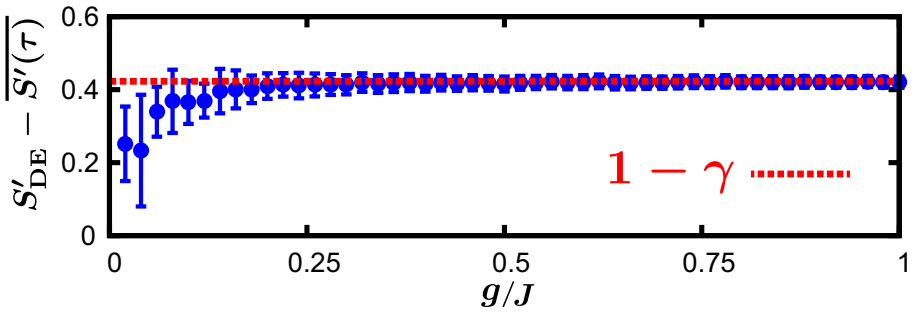

Figure 5.4: Numerical evidence for Conjecture 5.5. The difference $S'_{\rm DE} - \overline{S'(\tau)}$ is plotted for various magnitudes of the quench g/J. The error bars show the standard deviation of $S'(\tau)$ in τ. The data points are all below the bound $1-\gamma$ and equal to $1-\gamma$ independently of the quench magnitude for $g/J \gtrsim 0.25$.

we can measure the d-entropy. This method requires measurements only on diagonal elements of the density matrix while the ordinary method based on quantum tomography requires measurements on all the elements. Thus the universal-constant-based method has a practical advantage.

Chapter 6

Conclusions

In this thesis, we have addressed the foundation of statistical mechanics in isolated quantum systems from the first principles of quantum mechanics. In particular, we have focused on (i) why and how accurately the microcanonical ensemble describes equilibrium states and (ii) what microscopic definition describes the thermodynamic entropy. Once they are established, statistical mechanics is, as is well known, a very powerful tool with which we can calculate every physical quantity represented by a Hermitian operator by the microcanonical ensemble and every thermodynamic quantity such as the free energy by the microscopic definition of the thermodynamic entropy. However, answering to (i) and (ii) from quantum mechanics seems nontrivial due to, for example, the following three reasons. Firstly, if the initial state is a pure state, it remains pure in the course of subsequent time evolution, while the microcanonical ensemble is highly mixed. Secondly, the quantum-mechanical time evolution does not allow a state to converge to a fixed point in the Hilbert space. Finally, as for (ii), the von Neumann entropy, which has been used as the thermodynamic entropy in open quantum systems, is not consistent with the second law of thermodynamics if the time evolution including external operations is unitary.

In Chapters 2 and 3, we have reviewed some of the recent studies concerning this issue. It has been shown that even a pure state can represent thermal equilibrium in Chapter 2. The crucial idea is to restrict ourselves to few-body observables, which include all physical quantities that are measurable in ordinary experiments. Whereas a pure state can never be equal to the microcanonical ensemble as a quantum state that contains all the information including full N-body correlations, it can be so once we restrict the class of observables of interest. Furthermore, such a pure state has been shown to be typical in a microcanonical energy window. Namely, a pure state as a superposition of energy eigenstates in the window

is thermal with almost unit probability if it is taken according to the uniform Haar measure. In Chapter 3, equilibration has been understood by bringing together the two ideas introduced in Chapter 2: to restrict the observables of interest to few-body ones and to seek for a typical state among a set of quantum states. Here we have considered the set of states that appear in time evolution starting from an initial state instead of an artificial measure, the uniform Haar measure. As a consequence, we have shown that, starting from an initial state out of equilibrium, an effective stationary state can appear in time evolution. The effective stationary state thus derived explicitly depends on the memory of the initial state, the weight distribution on each energy eigenstate. We note that the microcanonical ensemble has an equal weight on each individual energy eigenstate in an energy window. Thus the former half of the question (i) reduces to why the weight distribution determined by the initial state plays no role in the stationary state. An answer to this question is that every eigenstate in a small energy window gives the same result in the thermodynamic limit when we restrict ourselves to few-body observables. This hypothesis is called the eigenstate thermalization hypothesis (ETH) and widely accepted since not a few pieces of numerical evidence have been obtained.

In Chapter 4, the latter half of the question (i) has been addressed. In finite-size systems, there are small errors for the microcanonical ensemble describing equilibrium states. We have first discussed that the ETH in finite-size systems gives two upper bounds (Eqs. (4.13) and (4.14)) on the accuracy of the microcanonical ensemble and shown that the accuracy improves at least as $D^{-1/2}$ with the dimension D of the Hilbert space. Since D grows exponentially in the degree of freedom in many-body systems, the improvement of the accuracy is also exponential. Then we have investigated the actual accuracy by conducting numerical experiments of quantum quenches in a nonintegrable one-dimensional model of hard-core bosons. As a result, it has turned out that the accuracy actually improves as D^{-1} which is much faster than the ETH bounds (Fig. 4.3). The D^{-1} scaling is comprised of one $D^{-1/2}$ by the ETH and the other $D^{-1/2}$ by the law of large numbers due to the fact that there is no correlation between the weights on many-body energy eigenstates as well as between the weight distribution and the eigenstate expectation values. This implies that we cannot induce any correlation through a quantum quench in nonintegrable systems since the many-body energy eigenstates are intricate seen from a natural configurational basis.

In Chapter 5, we have addressed the other question (ii). We have first pointed out two problems of the von Neumann entropy when we adopt it as the microscopic definition of the thermodynamic entropy of the effective stationary states in isolated quantum systems. Namely, (a) the von Neumann entropy vanishes if the stationary state is pure regardless of the

energy, and (b) it is kept constant under any unitary external operations including non-quasi-static ones. Then we have introduced the diagonal entropy, which is the Shannon entropy in the energy eigenbasis. This entropy resolves the problem (a) and can be regarded as a generalization of the von Neumann entropy so that it also applies to effective stationary states in isolated quantum systems. Moreover, we have shown that the diagonal entropy also settles the issue (b): the diagonal entropy does not decrease upon an arbitrary external operation consistently with the second law of thermodynamics (Corollaries 1 and 2).

Although we have thus addressed the two key questions (i) and (ii) regarding the foundation of statistical mechanics in isolated quantum systems, there are more related questions that can easily be raised. First, the ETH is still a hypothesis and has not been fully proven in any concrete model. The difficulty lies in the fact that the ETH holds only in nonintegrable models that are literally unsolvable. Second, the D^{-1} scaling of the accuracy of the microcanonical ensemble has been shown in a single numerical experiment and the universality should be investigated. Now that isolated quantum systems with a small number of atoms are available, this problem can also be tackled experimentally. Third, the uniqueness of the microscopic definition of the thermodynamic entropy is a completely open question. We have shown that non-decreasing function is possible as the diagonal entropy but never excluded other definitions. If we also consider open quantum systems and heat transfer, and require consistency with thermodynamics, we might be able to reach a unique microscopic definition of thermodynamic entropy. More and more questions can be raised since the foundation of statistical mechanics has been getting renewed attention only recently.

Appendix A

Wigner-Dyson statistics of energy level spacings

We cannot define chaos in quantum systems of finite degrees of freedom in a similar way in classical systems by using the sensitivity of the time evolution to the initial condition since the distance between any two wave functions is conserved under the unitary time evolution.

However, the energy spectrum of a quantum system behaves differently depending on whether or not its classical counterpart exhibits chaos. Namely, in a quantum system whose classical counterpart exhibits chaos, the difference between two adjacent eigenenergies obeys the Wigner-Dyson statistics. The probability distribution is well described by

$$p_{\mathrm{W}}(s) = \frac{\pi}{2} s \mathrm{e}^{-\frac{\pi}{4}s^2}, \tag{A.1}$$

where s denotes the normalized spacing between two adjacent eigenenergies so that the average of s is unity. This observation is called the BGS conjecture since Bohigas, Giannoni, and Schmit found it by analyzing quantum-mechanically the desymmetrized Sinai's billiard [96]. The BGS conjecture have been verified in a number of systems (see, *e.g.*, Ref. [97]).

The statement that the energy level spacings obey the Wigner-Dyson statistics can be tested within quantum mechanics and is used for checking if the quantum system of interest is nonintegrable. For example, Santos and Rigol have shown, in one-dimensional models of hard-core bosons and spinless fermions, that the distribution of the energy level spacings changes from the Poisson distribution to the Wigner-Dyson one as we increase the integrability breaking interaction.It has been shown that thermalization occurs in such systems that the Wigner-Dyson distribution appears [60].

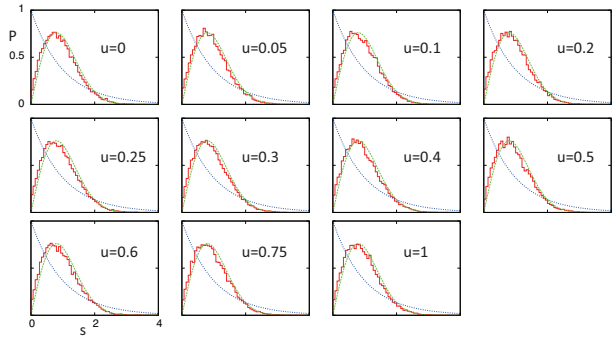

Figure A.1: The histograms of the normalized energy level spacings of the Hamiltonian (4.16). The dotted and dashed curves represent the Poisson $p(s) = \mathrm{e}^{-s}$ and the Wigner-Dyson (A.1) distributions, respectively. The data show better consistency with the latter.

We have confirmed that our Hamiltonian (4.16) gives the Wigner-Dyson statistics for the range of u used in the numerical experiments. Figure A.1 shows the histograms of the normalized level spacings at $L = 24$ for all the values u used in Chapter 4. For any u, the histograms are well described by the Wigner-Dyson distributions.

We describe the concrete procedure to obtain Fig. (A.1) before motivating each step. Following Ref. [98], we discard the two edges of the spectrum by 20% each and denote the remaining set of eigenvalues by $\{\epsilon_n\}_{n=0}^{d-1}$, which are arranged in an ascending order. Since there is no degeneracy in our model, the map $n \to \epsilon_n$ is strictly monotonically increasing. Thus, we define the inverse map denoted by $N(\epsilon)$ that is only defined at $\epsilon = \epsilon_n$ $(n = 0, 1, \ldots, d-1)$. Then, the least square fit with the 11th-order polynomial $f(\epsilon) = \sum_{r=0}^{11} a_r \epsilon^r$ has been done for $N(\epsilon)$ by GNUPLOT5.0. Then, we define $s_n = f(\epsilon_{n+1}) - f(\epsilon_n)$ $(n = 0, 1, \ldots, d-2)$, whose histogram is depicted in Fig. A.1.

We now motivate each step. First, truncating the two edges of the spectrum makes the result clearer because the fluctuations of the energy level spacings are large there. Second, transforming $\{\epsilon_n\}_{n=0}^{d-1}$ into $\{f(\epsilon_n)\}_{n=0}^{d-1}$ amounts to a normalization of $\{\epsilon_n\}_{n=0}^{d-1}$ so that the local average spacings are uniform in a wide range of the spectrum. If we directly analyzed the level spacings $\epsilon_{n+1} - \epsilon_n$, it would become systematically smaller in the middle of the spectrum where the density of states reaches the maximum, and we could not treat different portions of the spectrum at the same time. We have confirmed that changing the truncation ratio by 5% and the degree of the polynomial to the 13th in the fitting function do not qualitatively affect Fig. (A.1).

Appendix B

Statistical methods

This appendix supplements the concrete procedure which is used in Chapter 4. In Sec. B.1, we show how we have assigned the error bar to the root mean square of $\langle \hat{O} \rangle_{\mathrm{DE}} - \langle \hat{O} \rangle_{\mathrm{ME}}$ obtained for various initial states. In Sec. B.2, we describe how we have conducted the weighted nonlinear least squares (NLLS) fittings and obtained the confidence intervals.

B.1 Estimation error of RMS

For convenience, we consider the mean square (MS) instead of the root mean square (RMS). The latter is obtained by taking the square root of the former.

Let us denote by $\{x_i\}_{i=1}^n$ the set of $\langle \hat{O} \rangle_{\mathrm{DE}} - \langle \hat{O} \rangle_{\mathrm{ME}}$ obtained for each of the initial states for a given system size and a quench magnitude u_{f}, where n is the total number of the initial state. Then we define the MS by

$$\mathrm{MS} \equiv M^2 + V, \tag{B.1}$$

where M and V denote, respectively, the sample mean and the sample variance of the data:

$$M \equiv \frac{1}{n} \sum_{i=1}^{n} x_i; \tag{B.2}$$

$$V \equiv \frac{1}{n-1} \sum_{i=1}^{n} (x_i - M)^2. \tag{B.3}$$

The philosophy behind those definitions is the unbiased estimation of a virtual population, from which our samples $\{x_i\}_{i=1}^n$ were taken. The virtual population would be something

like a Gaussian distribution, a skewed Gaussian distribution, or something else, depending on the observable of interest as shown in Fig. (4.1)(b) and (d). For smaller system sizes, we suppose similar populations, which look rather obscure due to the small numbers of available samples. The definitions (B.1), (B.2), and (B.3), have been introduced with the idea that we estimate the MS of the virtual population unbiasedly. Let μ and σ^2 be the mean and variance of the population. Then the MS of the population is equal to $\mu^2 + \sigma^2$. Equations (B.2) and (B.3) are the unbiased estimations for μ and σ^2, which lead to Eq. (B.1). Rigorously speaking, the unbiasedness of estimators are expressed in terms of random variables $X_1, X_2, \ldots, X_n$, which are independent and identically distributed and have the common mean and variance, μ and σ^2. Namely, we regard $\{x_i\}_{i=1}^n$ as one realization of the set of n random variables even though more than one realization can never be obtained in reality. The functions of the random variables,

$$\mu_{\text{est}}(\{X_i\}) \equiv \frac{1}{n}\sum_{i=1}^{n} X_i \tag{B.4}$$

and

$$\sigma^2_{\text{est}}(\{X_i\}) \equiv \frac{1}{n-1}\sum_{i=1}^{n}[X_i - \mu_{\text{est}}(\{X_i\})]^2 \tag{B.5}$$

are the unbiased estimators for μ and σ^2, respectively, in the sense that

$$\langle \mu_{\text{est}}(\{X_i\})\rangle = \mu \quad \text{and} \quad \left\langle \sigma^2_{\text{est}}(\{X_i\})\right\rangle = \sigma^2 \tag{B.6}$$

where $\langle\cdots\rangle$ denotes the statistical averages over $X_1, X_2, \ldots, X_n$. Following these ideas, we have introduced the definitions (B.2) and (B.3) that correspond to Eqs. (B.4) and (B.5).

The estimations of μ and σ^2 are done unbiasedly but, of course, probabilistically distribute around μ and σ^2, respectively. We evaluate these estimation errors by the variances

$$\left\langle [\mu_{\text{est}}(\{X_i\}) - \mu]^2 \right\rangle = \frac{\sigma^2}{n} \tag{B.7}$$

and

$$\left\langle \left[\sigma^2_{\text{est}}(\{X_i\}) - \sigma^2\right]^2 \right\rangle = \frac{1}{n}\left\langle (X_j - \mu)^4 \right\rangle - \frac{n-3}{n(n-1)}\sigma^4, \tag{B.8}$$

respectively. We note that these variances are represented by the second and fourth moments

of the virtual population and thus have to be estimated from our data $\{x_i\}_{i=1}^n$.

The estimation of the right-hand side of Eq. (B.7) has already been done by Eq. (B.5). Thus we assign the estimation error of M as

$$\text{variance of } M = \frac{V}{n}. \tag{B.9}$$

The estimation of the right-hand side of Eq. (B.8) requires us to estimate the fourth moment of the virtual pupulation. We introduce a trial estimator

$$\omega_{\text{est}}(\{X_i\}) \equiv \frac{1}{n}\sum_i \left[X_i - \mu_{\text{est}}(\{X_i\})\right]^4. \tag{B.10}$$

A tedious calculation leads to

$$\langle \omega_{\text{est}}(\{X_i\})\rangle = \frac{(n-1)(n^2-3n+3)}{n^3}\left\langle (X_j-\mu)^4\right\rangle + \frac{3(n-1)(2n-3)}{n^3}\sigma^4. \tag{B.11}$$

Although the trial estimator (B.10) is biased, the bias can be "calibrated". Namely, combining Eqs. (B.8) and (B.11) and eliminating $\langle (X_j-\mu)^4\rangle$, we obtain

$$\left\langle \left[\sigma^2_{\text{est}}(\{X_i\}) - \sigma^2\right]^2\right\rangle = \frac{1}{(n-1)(n^2-3n+3)}\left[n^2\left\langle \omega_{\text{est}}(\{X_i\})\right\rangle - (n^2-3)\sigma^4\right]. \tag{B.12}$$

Thus we assign the estimation error of V as

$$\text{variance of } V = \frac{1}{(n-1)(n^2-3n+3)}\left[n\sum_{i=1}^n (x_i-M)^4 - (n^2-3)V^2\right] \equiv W. \tag{B.13}$$

Finally, the estimation error of the MS (B.1) is assigned through the chain rule of error propagation:

$$\text{Variance of MS} = 4M^2\frac{V}{n} + W \equiv \tilde{V}. \tag{B.14}$$

For example, in Fig. 4.2(a), the data points show the square root of Eq. (B.1) and the error bars ranging from the square root of $(\text{MS} - \tilde{V})^{1/2}$ to that of $(\text{MS} + \tilde{V})^{1/2}$.

B.2 Nonlinear least squares fit

Here we describe how we have fitted the data given in Fig. 4.2(a) and extracted the exponent with the confidence interval. Let us denote by $\{(x_i, y_i)\}_{i=1}^n$ the data to be fitted by a function $f(x)$, where i labels each data, n is the total number of the data, and $f(x)$ contains some fitting parameters. We assume that each y_i is accompanied by its variance σ_i^2. For our data in Fig. 4.2(a), we have $4\ (=n)$ data, $x_1 = 200$, $x_2 = 1026$, $x_3 = 5537$, and $x_4 = 30624$, and y_i and σ_i^2 are obtained by Eqs. (B.1) and (B.14), respectively. We have fitted these data by $f(x) = ax^b$ with two fitting parameters a and b.

We determine the best sets of the parameters a and b to minimize

$$\chi^2(a,b) = \sum_{i=1}^{n} \frac{1}{\sigma_i^2}(y_i - ax_i^b)^2, \tag{B.15}$$

which is the method of maximum likelihood for Gaussian variables [99]. We assume that each of our data $\{y_i\}_{i=1}^4$ obeys a Gaussian distribution since they consist of many data[1].

The minimization about a is analytically performed since Eq. (B.15) is quadratic with respect to the parameter. Namely, we have

$$\tilde{\chi}^2(b) = \min_a \chi^2(a,b) = \chi^2(a_*,b) = \sum_i \frac{y_i^2}{\sigma_i^2} - \frac{(\sum_i \frac{y_i x_i^b}{\sigma_i^2})^2}{\sum_i \frac{x_i^{2b}}{\sigma_i^2}}, \quad \left(a_* = \frac{\sum_i \frac{y_i x_i^b}{\sigma_i^2}}{\sum_i \frac{x_i^{2b}}{\sigma_i^2}} \right). \tag{B.16}$$

The minimization of b has been numerically done by solving

$$\frac{\mathrm{d}}{\mathrm{d}b}\tilde{\chi}^2(b)\bigg|_{b=b_*} = 0 \tag{B.17}$$

with Newton's method.

The confidence interval of b is obtained by assuming that $\tilde{\chi}^2(b) - \tilde{\chi}^2(b_*)$ obeys the chi-squared distribution with one degree of freedom [100]. To obtain the 95% confidence interval, for example, we find b_+ and b_- $(b_- < b_+)$ such that $\tilde{\chi}^2(b) - \tilde{\chi}^2(b_*) = 7.87944$. Then, the 95% confidence interval is obtained as $[b_-, b_+]$.

Finally, we divide b_*, b_+, and b_- by two to obtain the exponent and its confidence interval in the power-law decay of the RMS since it is obtained from the MS as its square root.

[1] We would expect that each y_i obeys the chi-squared distribution, which is approximated by the Gaussian distribution when the degrees of freedom are large.

Appendix C

Mathematical details for the d-entropy increase

In this Appendix, mathematical details for the results shown in Sec. 5.3 are supplemented. In Sec. C.1.1, we show two lemmas to prove Theorems 3 and 4 presented in Sec. 5.3.2. In Sections C.1.2 and C.1.3, we prove Theorems 3 and 4, respectively. Then we show, in Sec. C.2, that R is, under Assumption 3 in Sec 5.3.3, exponentially small in the number of sites. For the sake of simplicity, we set the Planck and Boltzmann constants, $\hbar$ and k_B, to unity throughout Appendix.

C.1 Proofs of Theorems

Without loss of generality, we assume $\mu_n > 0$ in the following discussion, where

$$\mu_n \equiv \sum_k |U_{nk}|^2 \rho^0_{kk}. \tag{C.1}$$

This is because n such that $\mu_n = 0$ does not contribute to the d-entropy after the operation which is given by

$$S'(\tau) \equiv -\sum_n \rho'_{nn}(\tau) \ln \rho'_{nn}(\tau), \tag{C.2}$$

where

$$\rho'_{nn}(\tau) = \sum_{k,l} U_{nk} U^*_{nl} \mathrm{e}^{-\mathrm{i}(E_k - E_l)\tau} \rho^0_{kl} \tag{C.3}$$

and τ denotes the time at which the external operation is performed. To see this fact, let us suppose that μ_n vanishes for an n. Then, Eq. (C.1) implies that $U_{nk} = 0$ or $\rho^0_{kk} = 0$ holds for all k. Here we note that, if $\rho^0_{kk} = 0$, then $\rho^0_{kl} = 0$ for all l because

$$|\rho^0_{kl}|^2 \leq \rho^0_{kk} \rho^0_{ll}, \tag{C.4}$$

follows from the fact that the density matrix $\hat{\rho}^0$ is positive-semidefinite[1]. Thus it follows from Eq. (C.3) that $\rho'_{nn}(\tau) = 0$ for all τ and this does not contribute to Eq. (C.2). In the following discussion, we hence assume that $\mu_n > 0$ without loss of generality.

C.1.1 Lemmas to prove Theorem 3, 4 and 5

Here we show two useful lemmas to prove Theorems 3 and 4 presented in Sec. 5.3.2 and Theorem 5 stated in Sec. C.2 below. Lemma 2 evaluates the long-time averages of $\rho'_{nn}(\tau)$ and its correlation over τ and Lemma 3 gives upper bounds on the correlation.

Lemma 2.

$$\overline{\rho'_{nn}(\tau)} = \mu_n; \tag{C.5}$$

$$\overline{\rho'_{mm}(\tau)\rho'_{nn}(\tau)} = \mu_m \mu_n + \nu_{mn}, \tag{C.6}$$

where

$$\nu_{mn} \equiv \sum_{\substack{k,l \\ k \neq l}} U_{mk} U^*_{ml} U^*_{nk} U_{nl} |\rho^0_{kl}|^2. \tag{C.7}$$

[1] R. A. Horn and C. R. Johnson, *Matrix Analysis* (Cambridge University Press, 1990), pp. 398.

Proof. From Eq. (C.3), the left-hand sides of Eqs. (C.5) and (C.6) read

$$\overline{\rho'_{nn}(\tau)} = \sum_{k,l} U_{nk}U^*_{nl}\overline{\mathrm{e}^{-\mathrm{i}(E_k-E_l)\tau}}\rho^0_{kl}; \tag{C.8}$$

$$\overline{\rho'_{mm}(\tau)\rho'_{nn}(\tau)} = \sum_{i,j,k,l} U_{mi}U^*_{mj}U^*_{nk}U_{nl}\overline{\mathrm{e}^{-\mathrm{i}(E_i-E_j-E_k+E_l)\tau}}\rho^0_{ij}(\rho^0_{kl})^*. \tag{C.9}$$

Assumption 2 stated in Sec. 5.3.1 leads to

$$\overline{\mathrm{e}^{-\mathrm{i}(E_k-E_l)\tau}} = \delta_{kl}; \tag{C.10}$$

$$\overline{\mathrm{e}^{-\mathrm{i}(E_i-E_j-E_k+E_l)\tau}} = \delta_{ij}\delta_{kl} + \delta_{ik}\delta_{jl} - \delta_{ij}\delta_{jk}\delta_{kl}. \tag{C.11}$$

Substituting Eq (C.10) into Eq. (C.8), we obtain Eq. (C.5). Meanwhile, with Eq (C.11) substituted into Eq. (C.9), the first term on the right-hand side of Eq. (C.11) gives $\mu_m\mu_n$ and the other two terms give ν_{mn}. Thus, we have obtained Eq. (C.6). □

Lemma 3.

$$\nu_{mn} \le \tilde{\nu}_{mn} \le \mu_m\mu_n, \tag{C.12}$$

where

$$\tilde{\nu}_{mn} \equiv \sum_{k,l} U_{mk}U^*_{ml}U^*_{nk}U_{nl}|\rho^0_{kl}|^2. \tag{C.13}$$

Proof. Firstly, the inequality $\nu_{mn} \le \tilde{\nu}_{mn}$ follows from $\tilde{\nu}_{mn} - \nu_{mn} = \sum_k |U_{mk}|^2|U_{nk}|^2(\rho^0_{kk})^2 \ge 0$.

Secondly, we prove the inequality $\tilde{\nu}_{mn} \le \mu_m\mu_n$. We note that

$$\tilde{\nu}_{mn} = \frac{1}{2}\sum_{k,l}(U_{mk}U^*_{ml}U^*_{nk}U_{nl} + \text{c.c.})|\rho^0_{kl}|^2 \tag{C.14}$$

and

$$U_{mk}U^*_{ml}U^*_{nk}U_{nl} + \text{c.c.} \le |U_{mk}|^2|U_{nl}|^2 + |U_{ml}|^2|U_{nk}|^2, \tag{C.15}$$

which follows from $|U_{mk}U_{nl} - U_{ml}U_{nk}|^2 \geq 0$. Then we obtain, from (C.14) and (C.15),

$$\tilde{\nu}_{mn} \leq \frac{1}{2}\sum_{k,l}(|U_{mk}|^2|U_{nl}|^2 + |U_{ml}|^2|U_{nk}|^2)|\rho^0_{kl}|^2 \tag{C.16}$$

$$\leq \sum_{k,l}|U_{mk}|^2|U_{nl}|^2\rho^0_{kk}\rho^0_{ll} \tag{C.17}$$

$$= \mu_m\mu_n, \tag{C.18}$$

where we used (C.4) to obtain (C.18). □

C.1.2 Proof of Theorem 3

We begin by showing the following lemma to prove Theorem 3.

Lemma 4. Let D be an arbitrary positive integer and $\{p_n\}$ and $\{q_n\}$ be sets of D real numbers satisfying $p_n \geq 0$ and $q_n > 0$ for $n = 1, 2, \ldots, D$ and $\sum_n p_n = \sum_n q_n = 1$. Then, the following inequalities hold:

$$0 \leq \sum_n p_n \ln\frac{p_n}{q_n} \leq \sum_n \frac{p_n^2}{q_n} - 1. \tag{C.19}$$

Proof. This lemma follows if we have

$$p_n - q_n \leq p_n \ln\frac{p_n}{q_n} \leq \frac{p_n^2}{q_n} - p_n, \tag{C.20}$$

because (C.20) reduces to (C.19) when summed over n. The proof of (C.20) is as follows. Since (C.20) trivially holds for $p_n = 0$, we assume $p_n > 0$. We note that $\ln x \leq x - 1$ holds for any $x > 0$. Substituting p_n/q_n and q_n/p_n for x, we obtain $1 - \frac{q_n}{p_n} \leq \ln\frac{p_n}{q_n} \leq \frac{p_n}{q_n} - 1$, which becomes (C.20) when multiplied by $p_n > 0$. □

Now we prove Theorem 3 by invoking Lemma 4.

Proof of Theorem 3. We substitute $\{\rho'_{nn}(\tau)\}$ and $\{\mu_n\}$ for $\{p_n\}$ and $\{q_n\}$, respectively, in Lemma 4, obtaining

$$0 \leq -\sum_n \rho'_{nn}(\tau)\ln\mu_n - S'(\tau) \leq \sum_n \frac{\rho'_{nn}(\tau)^2}{\mu_n} - 1, \tag{C.21}$$

where we used Eq. (C.2). By taking the long-time average of each side of (C.21) and using Eq. (C.5), we have

$$0 \leq S'_{\rm DE} - \overline{S'(\tau)} \leq \sum_n \frac{\overline{\rho'_{nn}(\tau)^2}}{\mu_n} - 1, \tag{C.22}$$

where $S'_{\rm DE} \equiv -\sum_n \mu_n \ln \mu_n$. Here we note that the inequality $\overline{\rho'_{nn}(\tau)^2} \leq 2\mu_n^2$ is obtained by Lemmas 2 and 3. Substituting this inequality into (C.22) and using $\sum_n \mu_n = 1$, we obtain

$$0 \leq S'_{\rm DE} - \overline{S'(\tau)} \leq 1. \tag{C.23}$$

Finally, we discuss the two equality conditions in (C.23). The equality on the right-hand side of (C.23) never holds since, the equality contradicts our assumption $\mu_n > 0$. In fact, the equality implies that $\nu_{nn} = \mu_n^2$ for any n, or $\sum_k |U_{nk}|^4 (\rho^0_{kk})^2 = 0$, and hence $\mu_n = 0$ for any n. The equality for the inequality on the left-hand side of Eq (C.23) holds, for example, if the initial state $\hat{\rho}^0$ is diagonal in the eigenbasis of $\hat{H}$ or if the transition matrix U_{mn} is diagonal. □

We point out that the term in the middle of (C.19) is known as the relative entropy or the Kullback-Leibler divergence:

$$D_{\rm KL}(\{p_n\}||\{q_n\}) \equiv \sum_n p_n \ln(p_n/q_n). \tag{C.24}$$

Thus, we have

$$\overline{D_{\rm KL}(\{\rho'_{nn}(\tau)\}||\{\mu_n\})} = S'_{\rm DE} - \overline{S'(\tau)}. \tag{C.25}$$

C.1.3 Proof of Theorem 4

We begin by showing the following lemma.

Lemma 5.

$$\overline{[S'(\tau) - S'_{\rm DE}]^2} \leq 2S'_{\rm DE} + R, \tag{C.26}$$

where

$$R \equiv \sum_{m,n} \nu_{mn} \ln \mu_m \ln \mu_n. \tag{C.27}$$

Proof. From the inequality on the left-hand side in (C.21), we have $S'(\tau) \leq -\sum_n \rho'_{nn}(\tau) \ln \mu_n$. Since $S'(\tau)$ is non-negative by definition, we have $S'(\tau)^2 \leq \sum_{m,n} \rho'_{mm}(\tau)\rho'_{nn}(\tau) \ln \mu_m \ln \mu_n$. Using Lemmas 2 and 3, we have

$$\overline{S'(\tau)^2} \leq \sum_{m,n} \overline{\rho'_{mm}(\tau)\rho'_{nn}(\tau)} \ln \mu_m \ln \mu_n \leq (S'_{\rm DE})^2 + R. \tag{C.28}$$

Finally, we obtain, by using (C.23) and (C.28),

$$\overline{\left[S'(\tau) - S'_{\rm DE}\right]^2} = \overline{S'(\tau)^2} - 2\overline{S'(\tau)}S'_{\rm DE} + (S'_{\rm DE})^2 \tag{C.29}$$

$$\leq 2S'_{\rm DE} + R. \tag{C.30}$$

□

Next, we show the following lemma, which is akin to Chebyshev's inequality.

Lemma 6.

$$\mathrm{Prob}\left[|S'_{\rm DE} - S'(\tau)| \geq C\right] \leq \frac{\overline{\left[S'(\tau) - S'_{\rm DE}\right]^2}}{C^2}, \tag{C.31}$$

where C is an arbitrary positive number.

Proof. We define

$$\theta(\tau) \equiv \begin{cases} 1 & \text{for } |S'_{\rm DE} - S'(\tau)| \geq C, \\ 0 & \text{for } |S'_{\rm DE} - S'(\tau)| < C, \end{cases} \tag{C.32}$$

which satisfies

$$\theta(\tau) \leq \frac{\left[S'_{\rm DE} - S'(\tau)\right]^2}{C^2}. \tag{C.33}$$

Taking the long-time averages of both sides of (C.33), we obtain (C.31). □

Proof of Theorem 4. From Lemma 5 and Lemma 6 with $C = S_0^{2/3}$, we have

$$\mathrm{Prob}\left[|S'_{\rm DE} - S'(\tau)| \geq S_0^{2/3}\right] \leq \frac{2S'_{\rm DE}}{S_0^{4/3}} + \frac{R}{S_0^{4/3}}. \tag{C.34}$$

Then, we obtain

$$\begin{aligned}
1 - \frac{2S'_{\rm DE}}{S_0^{4/3}} - \frac{R}{S_0^{4/3}} &\leq \mathrm{Prob}\left[|S'_{\rm DE} - S'(\tau)| < S_0^{2/3}\right] \\
&= \mathrm{Prob}\left[S'_{\rm DE} - S_0^{2/3} < S'(\tau) < S'_{\rm DE} + S_0^{2/3}\right] \\
&\leq \mathrm{Prob}\left[S'_{\rm DE} - S_0^{2/3} < S'(\tau)\right] \\
&\leq \mathrm{Prob}\left[S_0 - S_0^{2/3} < S'(\tau)\right], \qquad \text{(C.35)}
\end{aligned}$$

where we used $S_0 \leq S'_{\rm DE}$ to obtain the last inequality. □

C.2 The exponential smallness of R

In this section, we prove that R is exponentially small in N, or the number of sites of the lattice system if Assumption 2 introduced in Sec. 5.3.3 is satisfied, which dictates that an effective dimension is exponentially large in N:

$$D_{\rm eff} \equiv \left[\sum_n (\rho^0_{nn})^2\right]^{-1} = \mathrm{e}^{O(N)}. \qquad \text{(C.36)}$$

This result is a consequence of the following theorem.

Theorem 5.

$$R \leq \frac{5(\ln D)^2}{D_{\rm eff}^{1/2}} + \frac{8(\ln D)^2}{D} + \frac{4(\ln D)^2}{D^2} \qquad \text{(C.37)}$$

holds for any integer $D\,(\geq 2)$.

We note that Theorem 5 ensures, together with Eq. (C.36) and $D = d^N$, that R is exponentially small in N.

Proof. We note that Lemma 3 ensures that

$$R \leq \tilde{R} \equiv \sum_{m,n} \tilde{\nu}_{mn} \ln \mu_m \ln \mu_n. \qquad \text{(C.38)}$$

Thus it is sufficient to prove Theorem 5 for $\tilde{R}$ instead of R. We separate $\tilde{R}$ into two parts as

$$\tilde{R} = \sum_{(m,n)\in A\setminus B} \tilde{\nu}_{mn} \ln \mu_m \ln \mu_n + \sum_{(m,n)\in B} \tilde{\nu}_{mn} \ln \mu_m \ln \mu_n, \tag{C.39}$$

where the sets of indices, A and B, are defined as

$$A \equiv \{(m,n) \in \{1,\dots,D\} \times \{1,\dots,D\}\}; \tag{C.40}$$

$$B \equiv \{(m,n) \in A \mid D_{\text{eff}}^{-1/2} \mu_m \mu_n \le \tilde{\nu}_{mn} \le \mu_m \mu_n\}. \tag{C.41}$$

Here we note that $\tilde{\nu}_{mn} \le D_{\text{eff}}^{-1/2} \mu_m \mu_n$ holds for $(m,n) \in A \setminus B$ because Lemma 3 ensures $\tilde{\nu}_{mn} \le \mu_m \mu_n$ for any $(m,n) \in A$. Then the first term on the right-hand side of Eq. (C.39) is bounded from above as

$$\sum_{(m,n)\in A\setminus B} \tilde{\nu}_{mn} \ln \mu_m \ln \mu_n \le D_{\text{eff}}^{-1/2} \sum_{(m,n)\in A\setminus B} \mu_m \mu_n \ln \mu_m \ln \mu_n \tag{C.42}$$

$$\le D_{\text{eff}}^{-1/2} \sum_{(m,n)\in A} \mu_m \mu_n \ln \mu_m \ln \mu_n \tag{C.43}$$

$$= D_{\text{eff}}^{-1/2} S_{\text{DE}}'^2 \tag{C.44}$$

$$\le D_{\text{eff}}^{-1/2} (\ln D)^2. \tag{C.45}$$

Here we used $S'_{\text{DE}} \le \ln D$ in deriving the last inequality. Now the second term on the right-hand side of Eq. (C.39) is bounded from above as

$$\sum_{(m,n)\in B} \tilde{\nu}_{mn} \ln \mu_m \ln \mu_n \le \sum_{(m,n)\in B} \mu_m \mu_n \ln \mu_m \ln \mu_n. \tag{C.46}$$

We define three subsets of B as

$$B_1 = \{(m,n) \in B \mid \mu_m \ge D^{-2} \text{ and } \mu_n \ge D^{-2}\}, \tag{C.47}$$

$$B_2 = \{(m,n) \in B \mid \mu_m \ge D^{-2} \text{ and } \mu_n < D^{-2}\}, \tag{C.48}$$

$$B_3 = \{(m,n) \in B \mid \mu_m < D^{-2} \text{ and } \mu_n < D^{-2}\}, \tag{C.49}$$

and accordingly separate $\sum_{(m,n)\in B} \mu_m \mu_n \ln \mu_m \ln \mu_n$ into three parts $\tilde{R}_1 + 2\tilde{R}_2 + \tilde{R}_3$, where

$$\tilde{R}_\alpha \equiv \sum_{(m,n)\in B_\alpha} \mu_m \mu_n \ln \mu_m \ln \mu_n \quad (\alpha = 1,2,3). \tag{C.50}$$

Then,

$$\tilde{R} \leq D_{\text{eff}}^{-1/2}(\ln D)^2 + \tilde{R}_1 + 2\tilde{R}_2 + \tilde{R}_3. \tag{C.51}$$

We give upper bounds for each $\tilde{R}_\alpha$ $(\alpha = 1, 2, 3)$.

First, since $\ln \mu_m \ln \mu_n \leq 4(\ln D)^2$ for $(m, n) \in B_1$, we have

$$\tilde{R}_1 \leq 4(\ln D)^2 \sum_{(m,n)\in B_1} \mu_m \mu_n \leq 4D_{\text{eff}}^{-1/2}(\ln D)^2, \tag{C.52}$$

where the last inequality holds if the following inequality is satisfied:

$$\sum_{(m,n)\in B} \mu_m \mu_n \leq D_{\text{eff}}^{-1/2}. \tag{C.53}$$

To show this, we sum $D_{\text{eff}}^{-1/2}\mu_m\mu_n \leq \tilde{\nu}_{mn}$ over m and n such that $(m, n) \in B$, obtaining

$$D_{\text{eff}}^{-1/2} \sum_{(m,n)\in B} \mu_m \mu_n \leq \sum_{(m,n)\in B} \tilde{\nu}_{mn} \leq \sum_{m,n} \tilde{\nu}_{mn} = D_{\text{eff}}^{-1}, \tag{C.54}$$

where the last equality follows from $\sum_m U_{mk}U_{ml}^* = \delta_{kl}$. Multiplying (C.54) by $D_{\text{eff}}^{1/2}$, we obtain (C.53).

Second, noting that $-\mu_n \ln \mu_n \leq 2D^{-2} \ln D$ since $\mu_n < D^{-2} \leq 4$, we have

$$\tilde{R}_2 \leq \frac{4(\ln D)^2}{D^2} \sum_{(m,n)\in B_2} \mu_m \leq \frac{4(\ln D)^2}{D^2} \sum_{(m,n)\in A} \mu_m = \frac{4(\ln D)^2}{D}. \tag{C.55}$$

Finally, as we did for $\tilde{R}_2$, we have

$$\tilde{R}_3 \leq \frac{4(\ln D)^2}{D^4} \sum_{(m,n)\in B_3} 1 \leq \frac{4(\ln D)^2}{D^4} \sum_{(m,n)\in A} 1 = \frac{4(\ln D)^2}{D^2}. \tag{C.56}$$

Combining (C.38) (C.51), (C.52), (C.55), and (C.56), we eventually obtain (C.37). □

C.3 Derivation of the universal constant

In this section, we derive

$$S'_{\mathrm{DE}} - \overline{S'(\tau)} = 1 - \gamma \tag{C.57}$$

for a pure state when a unitary external operation causes numerous transitions between energy eigenstates.

Let $|\Psi^0\rangle$ be the pure initial state. Correspondingly, we have $\hat{\rho}^0 = |\Psi^0\rangle \langle\Psi^0|$.

Introducing the expansion coefficients $c_n \equiv \langle E_n|\Psi^0\rangle$ in the energy eigenbasis, we have

$$\rho^0_{mn} = c_m c^*_n. \tag{C.58}$$

The separability of the two indices, m and n, on the right-hand side of Eq. (C.58) is one of the characteristics of a pure state, which plays a crucial role in deriving the universal constant, $1 - \gamma$.

C.3.1 Moments of the population of each eigenstate after the operation

Here we discuss the statistical properties of the population of each eigenstate, $\rho'_{nn}(\tau)$, with τ obeys a uniform distribution. We calculate any order of the moments and show that it obeys an exponential distribution.

Let us analyze the moment of the k-th order:

$$\overline{[\rho'_{nn}(\tau)]^k} = \sum_{\substack{m_1,\ldots,m_k \\ l_1,\ldots,l_k}} \left[\prod_{j=1}^{k} U_{nm_j} U^*_{nl_j} c_{m_j} c^*_{l_j} \right] \overline{\mathrm{e}^{-\mathrm{i}\left(\sum_{j=1}^{k} E_{m_j} - \sum_{j=1}^{k} E_{l_j}\right)\tau}}. \tag{C.59}$$

To calculate the long-time average on the right-hand side of Eq. (C.59), we make the following assumption in addition to Assumption 2.

Assumption 4. For $k \geq 3$, $\overline{\mathrm{e}^{-\mathrm{i}\left(\sum_{j=1}^{k} E_{m_j} - \sum_{j=1}^{k} E_{l_j}\right)\tau}}$ equals 1 if $\{m_j\}_{j=1}^k$ is obtained by a permutation of $\{l_j\}_{j=1}^k$ and otherwise 0.

Assumption 4 leads to a generalization of Eq. (C.11), which is

$$\overline{\mathrm{e}^{-\mathrm{i}\left(\sum_{j=1}^{k} E_{m_j}-\sum_{j=1}^{k} E_{l_j}\right)\tau}} = \sum_{\sigma\in\mathcal{S}_k}\prod_{j=1}^{k}\delta_{m_j l_{\sigma(j)}} + (\text{corrections}), \tag{C.60}$$

where $\mathcal{S}_k$ is the symmetric group of order k and "corrections" stand for compensations for multiple counting, which involve more Kronecker's deltas than the first term on the right-hand side of Eq. (C.60).

We emphasize that if there are numerous transitions between energy eigenstates, "corrections" can be ignored when Eq. (C.60) is substituted into the right-hand side of Eq. (C.59). This is because the contributions from "corrections" are smaller roughly by a factor of $Q_n \equiv \sum_m \left(|U_{nm}|^2|c_m|^2\right)^2/\mu_n^2$ than that from the first term on the right-hand side of Eq. (C.60), where $\mu_n = \sum_m |U_{nm}|^2|c_m|^2$. Here Q_n^{-1} implies an effective number of m such that $|U_{nm}|^2|c_m|^2$ does not vanish, which is quite large when there are numerous transitions between energy eigenstates and $|U_{nm}|^2$ spreads over many m for a given n.

Substituting Eq. (C.60) with "corrections" ignored into Eq. (C.59), we obtain

$$\overline{[\rho'_{nn}(\tau)]^k} = k!\mu_n^k. \tag{C.61}$$

Equation (C.61) means that $\rho'_{nn}(\tau)$ obeys an exponential distribution

$$\begin{aligned}&\mathrm{Prob}[M_n \le \rho'_{nn}(\tau) \le M_n + \mathrm{d}M_n] \\ &\quad = \frac{\mathrm{e}^{-M_n/\mu_n}}{\mu_n}\mathrm{d}M_n \quad (M_n \ge 0),\end{aligned} \tag{C.62}$$

whose mean and variance are given by μ_n and μ_n^2, respectively.

C.3.2 Average of the entropy after the operation

In our approximation, the long-time average of $S'(\tau)$ is obtained by taking the average over the exponential distribution [Eq. (C.62)]:

$$\overline{S'(\tau)} = -\sum_n \int_0^\infty M_n \ln M_n \frac{\mathrm{e}^{-M_n/\mu_n}}{\mu_n}\mathrm{d}M_n. \tag{C.63}$$

This integration can be analytically performed to give

$$\begin{aligned}\overline{S'(\tau)} &= -\sum_n \mu_n \ln \mu_n + \gamma - 1 \\ &= S'_{\mathrm{DE}} + \gamma - 1, \end{aligned} \tag{C.64}$$

where γ is Euler's constant. It is noteworthy that the constant $\gamma - 1$ does not depend on the details of the system and the operation, whereas S'_{DE} does.

Finally, we provide yet another derivation of the universal constant $\gamma - 1$ by invoking the so-called replica trick [101]. This derivation makes it clear that the universal constant $\gamma - 1$ originates from the factorial $k!$ in Eq. (C.61), or, equivalently, from the quantum coherence between energy eigenstates. The replica trick relies on the analytic continuation of Eq. (C.61) to $k = 0$:

$$\begin{aligned}\overline{S'(\tau)} &= -\sum_n \lim_{k\to 0} \frac{\overline{\rho'_{nn}(\tau)^{k+1}} - \overline{\rho'_{nn}(\tau)}}{k} \\ &= -\sum_n \lim_{k\to 0} \frac{\Gamma(k+2)\mu_n^{k+1} - \mu_n}{k} \\ &= -\sum_n \mu_n \ln \mu_n + \gamma - 1, \end{aligned} \tag{C.65}$$

where we have used $\Gamma'(2) = 1 - \gamma$ to obtain the last equality. It is clear from this derivation that the universal constant arises from $k! = \Gamma(k+1)$.

Bibliography

[1] J. Gibbs, *Elementary principles in statistical mechanics : developed with especial reference to the rational foundation of thermodynamics*, Ox Bow Press, Woodbridge, Conn, 1981.

[2] L. Landau and E. Lifshitz, *Statistical Physics*, Number v. 5, Elsevier Science, 1996.

[3] H. Callen, *Thermodynamics and an introduction to thermostatistics*, Wiley, New York, 1985.

[4] L. Boltzmann, *Lectures on gas theory*, Dover Publications, New York, 1995.

[5] L. Onsager, Phys. Rev. **65**, 117 (1944).

[6] S. Chandrasekhar, Astrophys. J. **74**, 81 (1931).

[7] H. Tazaki, *Statistical Mechanics I (in Japanese)*, Baifukan, Tokyo, 2008.

[8] P. Ehrenfest, *The conceptual foundations of the statistical approach in mechanics*, Dover Publications, New York, 1990.

[9] G. D. Birkhoff, Proc. Natl. Acad. Sci. U. S. A. **17**, 656 (1931).

[10] Y. G. Sinai, Russ. Math. Surv. **25**, 137 (1970).

[11] Y. Oono, http://www.yoono.org/y_oono_official_site/statphysjogging.html.

[12] A. Shimizu, http://as2.c.u-tokyo.ac.jp/lecture_note.

[13] S. Goldstein, J. Lebowitz, R. Tumulka, and N. Zanghì, Phys. Rev. Lett. **96**, 050403 (2006).

[14] S. Popescu, A. J. Short, and A. Winter, Nat. Phys. **2**, 754 (2006).

[15] A. Sugita, RIMS Kokyuroku **1507**, 147 (2006).

[16] P. Reimann, Phys. Rev. Lett. **99**, 160404 (2007).

[17] P. Bocchieri and A. Loinger, Phys. Rev. **114**, 948 (1959).

[18] S. Lloyd, arXiv:1307.0378 (2013).

[19] J. von Neumann, Eur. Phys. J. H **35**, 201 (2010).

[20] A. Peres, Phys. Rev. A **30**, 504 (1984).

[21] P. Reimann, Phys. Rev. Lett. **101**, 190403 (2008).

[22] M. Rigol, V. Dunjko, and M. Olshanii, Nature **452**, 854 (2008).

[23] N. Linden, S. Popescu, A. Short, and A. Winter, Phys. Rev. E **79**, 061103 (2009).

[24] L. P. Pitaevskii, *Bose-Einstein condensation*, Clarendon Press, Oxford New York, 2003.

[25] C. Pethick, *Bose-Einstein condensation in dilute gases*, Cambridge University Press, Cambridge New York, 2008.

[26] A. J. Leggett, *Quantum liquids Bose condensation and Cooper pairing in condensed-matter systems*, Oxford University Press, Oxford New York, 2006.

[27] M. Ueda, *Fundamentals and new frontiers of Bose-Einstein condensation*, World Scientific, Singapore Hackensack, NJ, 2010.

[28] C. Cohen-Tannoudji, J. Dupont-Roc, and G. Grynberg, *Atom-photon interactions: basic processes and applications*, Wiley Online Library, 1992.

[29] M. H. Anderson, J. R. Ensher, M. R. Matthews, C. E. Wieman, and E. A. Cornell, Science **269**, 198 (1995).

[30] K. Davis et al., Phys. Rev. Lett. **75**, 3969 (1995).

[31] G. Raithel, G. Birkl, A. Kastberg, W. Phillips, and S. Rolston, Phys. Rev. Lett. **78**, 630 (1997).

[32] T. Müller-Seydlitz et al., Phys. Rev. Lett. **78**, 1038 (1997).

[33] S. Hamann et al., Phys. Rev. Lett. **80**, 4149 (1998).

[34] D. Jaksch and P. Zoller, Ann. Phys. (N. Y). **315**, 52 (2005).

[35] I. Buluta and F. Nori, Science **326**, 108 (2009).

[36] S. Trotzky et al., Nat. Phys. **8**, 325 (2012).

[37] T. Kinoshita, T. Wenger, and D. S. Weiss, Nature **440**, 900 (2006).

[38] M. Gring et al., Science **337**, 1318 (2012).

[39] J. Berges, S. Borsányi, and C. Wetterich, Phys. Rev. Lett. **93**, 142002 (2004).

[40] T. Langen, R. Geiger, M. Kuhnert, B. Rauer, and J. Schmiedmayer, Nat. Phys. **9**, 640 (2013).

[41] F. Serwane et al., Science **332**, 336 (2011).

[42] A. Polkovnikov, Ann. Phys. (N. Y). **326**, 486 (2011).

[43] D. Page, Phys. Rev. Lett. **71**, 1291 (1993).

[44] S. Sugiura and A. Shimizu, Phys. Rev. Lett. **108**, 240401 (2012).

[45] S. Sugiura and A. Shimizu, Phys. Rev. Lett. **111**, 010401 (2013).

[46] T. Monnai and A. Sugita, J. Phys. Soc. Japan **83**, 094001 (2014).

[47] R. Steinigeweg, A. Khodja, H. Niemeyer, C. Gogolin, and J. Gemmer, Phys. Rev. Lett. **112**, 130403 (2014).

[48] P. Bocchieri and A. Loinger, Phys. Rev. **107**, 337 (1957).

[49] W. Schmidt, *Diophantine approximation*, Springer-Verlag, Berlin New York, 1980.

[50] A. Peres, Phys. Rev. Lett. **49**, 1118 (1982).

[51] H. Tasaki, Phys. Rev. Lett. **80**, 1373 (1998).

[52] S. Goldstein, J. L. Lebowitz, R. Tumulka, and N. Zanghì, Eur. Phys. J. H **35**, 173 (2010).

[53] S. Goldstein, J. L. Lebowitz, C. Mastrodonato, R. Tumulka, and N. Zanghi, Proc. R. Soc. A Math. Phys. Eng. Sci. **466**, 3203 (2010).

[54] H. Tasaki, arXiv:1003.5424v4 , 27 (2010).

[55] A. J. Short, New J. Phys. **13**, 053009 (2011).

[56] J. Deutsch, Phys. Rev. A **43**, 2046 (1991).

[57] M. Srednicki, Phys. Rev. E **50**, 888 (1994).

[58] M. Horoi, V. Zelevinsky, and B. Brown, Phys. Rev. Lett. **74**, 5194 (1995).

[59] M. Rigol, Phys. Rev. A **80**, 053607 (2009).

[60] M. Rigol and L. F. Santos, Phys. Rev. A **82**, 8 (2010).

[61] L. F. Santos and M. Rigol, Phys. Rev. E **82**, 031130 (2010).

[62] W. Beugeling, R. Moessner, and M. Haque, Phys. Rev. E **89**, 042112 (2014).

[63] H. Kim, T. N. Ikeda, and D. A. Huse, Phys. Rev. E **90**, 052105 (2014).

[64] A. Khodja, R. Steinigeweg, and J. Gemmer, Phys. Rev. E **91**, 012120 (2015).

[65] A. Pal and D. A. Huse, Phys. Rev. B **82**, 174411 (2010).

[66] C. Gogolin, M. P. Müller, and J. Eisert, Phys. Rev. Lett. **106**, 040401 (2011).

[67] M. Rigol and M. Srednicki, Phys. Rev. Lett. **108**, 5 (2011).

[68] T. N. Ikeda, Y. Watanabe, and M. Ueda, Phys. Rev. E **84**, 021130 (2011).

[69] P. Grisins and I. E. Mazets, Phys. Rev. A **84**, 053635 (2011).

[70] T. Ikeda, Y. Watanabe, and M. Ueda, Phys. Rev. E **87**, 012125 (2013).

[71] M. Rigol, V. Dunjko, V. Yurovsky, and M. Olshanii, Phys. Rev. Lett. **98**, 4 (2006).

[72] E. Jaynes, Phys. Rev. **106**, 620 (1957).

[73] M. Cazalilla, Phys. Rev. Lett. **97**, 156403 (2006).

[74] P. Calabrese and J. Cardy, J. Stat. Mech. Theory Exp. **2007**, P06008 (2007).

[75] A. Iucci and M. A. Cazalilla, Phys. Rev. A **80**, 063619 (2009).

[76] A. C. Cassidy, C. W. Clark, and M. Rigol, Phys. Rev. Lett. **106**, 140405 (2010).

[77] P. Calabrese, F. H. L. Essler, and M. Fagotti, Phys. Rev. Lett. **106**, 227203 (2011).

[78] M. Kollar, F. A. Wolf, and M. Eckstein, Phys. Rev. B **84**, 054304 (2011).

[79] M. A. Cazalilla, A. Iucci, and M.-C. Chung, Phys. Rev. E **85**, 011133 (2012).

[80] B. Pozsgay, J. Stat. Mech. Theory Exp. **2013**, P07003 (2013).

[81] M. Fagotti and F. H. L. Essler, J. Stat. Mech. Theory Exp. **2013**, P07012 (2013).

[82] J. Mossel and J.-S. Caux, New J. Phys. **14**, 075006 (2012).

[83] M. Mierzejewski, P. Prelovšek, and T. Prosen, Phys. Rev. Lett. **113**, 020602 (2014).

[84] M. Kormos, A. Shashi, Y.-Z. Chou, J.-S. Caux, and A. Imambekov, Phys. Rev. B **88**, 205131 (2013).

[85] M. Moeckel and S. Kehrein, Phys. Rev. Lett. **100**, 175702 (2008).

[86] M. Moeckel and S. Kehrein, Ann. Phys. (N. Y). **324**, 2146 (2009).

[87] M. Moeckel and S. Kehrein, New J. Phys. **12**, 055016 (2010).

[88] V. Lazutkin, *KAM Theory and Semiclassical Approximations to Eigenfunctions*, Springer Berlin Heidelberg, Berlin, Heidelberg, 1993.

[89] V. Alba, arXiv:1409.6096 (2014).

[90] T. N. Ikeda, N. Sakumichi, A. Polkovnikov, and M. Ueda, page 8 (2013).

[91] M. Nielsen and I. Chuang, *Quantum computation and quantum information*, Cambridge University Press, Cambridge New York, 2010.

[92] J. Neumann, *Mathematical foundations of quantum mechanics*, Princeton University Press, Princeton N.J, 1955.

[93] C. E. Shannon, Bell Syst. Tech. J. **27**, 379 (1948).

[94] A. Lenard, J. Stat. Phys. **19**, 575 (1978).

[95] H. Tasaki, arXiv:cond-mat/0011321v2 (2000).

[96] O. Bohigas, M. Giannoni, and C. Schmit, Phys. Rev. Lett. **52**, 1 (1984).

[97] Stöckmann, *Quantum chaos*, Cambridge University Press, Cambridge, 2006.

[98] L. F. Santos and M. Rigol, Phys. Rev. E **81**, 036206 (2010).

[99] P. Bevington, *Data reduction and error analysis for the physical sciences*, McGraw-Hill, Boston, 2003.

[100] M. Bonamente, *Statistics and analysis of scientific data*, Springer, New York, NY, 2013.

[101] S. F. Edwards and P. W. Anderson, J. Phys. F Met. Phys. **5**, 965 (1975).